

Persistent spin currents in superconducting altermagnets

Kyle Monkman,¹ Joan Weng,¹ Niclas Heinsdorf,^{1,2} Alberto Nocera,¹ and Marcel Franz¹

¹*Department of Physics and Astronomy, and Quantum Matter Institute,
University of British Columbia, Vancouver, BC, Canada V6T 1Z1*

²*Max Planck Institute for Solid State Research, Heisenbergstrasse 1, 70569 Stuttgart, Germany*
(Dated: July 31, 2025)

Superconductors are famously capable of supporting persistent electrical currents, that is, currents that flow without any measurable decay as long as the material is kept in the superconducting state. We introduce here a class of materials – superconducting altermagnets – that can both generate and carry persistent *spin* currents. This includes spin-polarized electrical supercurrent as well as pure spin supercurrent that facilitates spin transport in the absence of any charge transport. A key to this remarkable property is the realization that the leading superconducting instability of altermagnetic metals consists of two independent condensates formed of spin-up and spin-down electrons. In the non-relativistic limit the two condensates are decoupled and can thus naturally support persistent currents with any spin polarization, including pure spin supercurrents realized in the charge counterflow regime. We describe a novel “spin-current dynamo effect” that can be used to generate pure spin supercurrent in such systems by driving a charge current along certain crystallographic directions. Away from the non-relativistic limit, when spin-orbit interactions and magnetic disorder are present, we find that the spin current generically develops spatial oscillations but, importantly, no dissipation or decay. This is in stark contrast to spin currents in normal diffusive metals which tend to decay on relatively short lengthscales. We illustrate the above properties by performing model calculations relevant to two distinct classes of altermagnets and various device geometries.

I. INTRODUCTION

The magic of supercurrent lies in the fact that it flows in the ground state of the system. In some geometries, such as a superconducting (SC) ring threaded by magnetic flux that is some fraction of the SC flux quantum $\Phi_0 = hc/2e$, the current cannot decay even as a matter of principle, simply because it flows in the quantum state with the lowest energy [1, 2]. As a more practical matter the fact that persistent currents are not subject to dissipation has been widely exploited in devices, e.g. to generate magnetic fields for a broad range of applications. Quantum coherence of the SC condensate also forms a basis for an important class of qubits and quantum sensors based on the ubiquitous Josephson effect.

Unlike electric charge, spin is generically not conserved in solids. Transporting spin over long enough distances so that it can be successfully manipulated and read out is one of the key requirements of spintronics [3, 4]. In diffusive normal metals and semiconductors spin lifetimes are typically quite short owing to the spin-orbit coupling (SOC) and spin-flip scattering. The quest in the spintronic community to remedy this situation has led to the advent of superconducting spintronics [5, 6] which seeks to exploit dissipationless currents carried by superconductors to achieve long spin transport lifetimes. This effort has produced a number of notable advances [7–10] and has culminated in the recent demonstration of a tunable pure spin supercurrent in heterostructures composed of a ferromagnet, spin-orbit coupled metal and a conventional superconductor such as Pt/Co/Pt/Nb/Ni₈Fe₂ [11]. Additionally, a number of theoretical proposals have been advanced aimed at improving performance and attaining

new functionalities in superconducting spintronic devices [12–16].

Despite this progress, platforms that combine superconductors with ferromagnets have some inescapable drawbacks: Ferromagnets produce stray fields that can lead to undesirable coupling between distant circuit elements. Also, conventional superconducting order tends to be strongly suppressed by the magnetic field through both orbital and Zeeman depairing. Likewise, magnetic exchange coupling is pair-breaking for conventional spin-singlet Cooper pairs. As a result, it would be vastly preferable if one could generate and sustain spin-polarized persistent currents in structures with zero net magnetization. In what follows, we discuss one such platform based on the recently discovered family of altermagnetic metals [17–22]. Similar to antiferromagnets, altermagnets exhibit zero net magnetization enforced by their spin group symmetry [23–28]. Nevertheless they possess spin-split fermi surfaces which, as we will demonstrate, are naturally suited to form a basis for exotic equal-spin triplet SC order capable of both generating and supporting persistent spin currents.

The reason for this is quite simple and can be readily understood from Fig. 1 which depicts spin-split fermi surfaces typical of two families of altermagnets with 4-fold and 6-fold rotation symmetry, also known as *d*- and *g*-wave altermagnets. We observe that these types of fermi surfaces are fundamentally incompatible with the conventional spin-singlet superconducting instability: for a spin-up electron at crystal momentum $+\mathbf{k}$ there is no requisite spin-down electron available at $-\mathbf{k}$. Instead, a zero-momentum Cooper pair must form from two electrons with equal spin, which also necessitates odd-parity

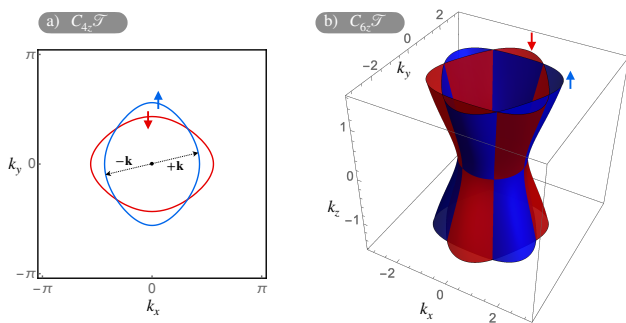


FIG. 1. Spin split Fermi surfaces of (a) d -wave and (b) g -wave altermagnetic metals described by Hamiltonians Eq. (1) and (3) for altermagnetic band splitting parameter $\eta = 0.2$. Blue and red color distinguishes up and down spin projections.

spatial symmetry of the pair wave function $g_{\mathbf{k}} = -g_{-\mathbf{k}}$. This intuition has recently been formalized by a general group-theoretic classification of symmetry-allowed SC phases in altermagnets [29] which highlighted spin-triplet order parameters as most natural SC instabilities.

Importantly for the task at hand, in the strictly non-relativistic limit (that is, in the absence of SOC) the two spin species are decoupled and so are the two superconducting condensates. It is this feature that ultimately enables all the interesting spintronic properties of such condensates discussed below. For example, one could imagine setting up superflow in spin-up condensate only: the resulting persistent current would then be fully spin-polarized. Likewise, a state with the two condensates flowing in the opposite direction realizes a pure spin supercurrent, transporting spin with no concomitant charge transport.

In normal metals, inclusion of SOC and spin-flip scattering is known to lead to short spin lifetimes, which are often the main limiting factors in spintronics devices [3]. An important question therefore arises as to the effect of such perturbations on the efficacy of the proposed new platform. To address this question we perform an extensive analysis in the framework of microscopic models as well phenomenological Ginzburg-Landau (GL) theory and show that SOC does not destroy these behaviors unless its strength exceeds a critical value. Specifically, we find that inclusion of SOC causes spatial oscillations in spin supercurrent amplitude along the flow direction, but, crucially, no decay or dissipation. Hence, superconducting altermagnets can carry persistent spin currents over long distances even when SOC is present. We also explore the effect of spin-flip scattering caused by magnetic disorder and find that unless it is very strong (so as to significantly suppress the SC order) it also does not substantially degrade the spin supercurrent.

As argued previously [30–34] the leading SC instability of a d -wave altermagnet in the presence of a weak attractive interaction occurs in the equal-spin triplet channel with a fully gapped $p_x \pm ip_y$ order parameter. This is relevant to altermagnets with the square-lattice symme-

try including the recently discovered quasi-2D oxychalcogenide metals $\text{KV}_2\text{Se}_2\text{O}$ [22] and $\text{Rb}_{1-\delta}\text{V}_2\text{Te}_2\text{O}$ [35]. In the following we perform the same type of analysis for g -wave altermagnets and show that the leading SC instability also occurs in the equal-spin triplet $p_x \pm ip_y$ channel. This is potentially relevant to a number of confirmed altermagnets with the hexagonal symmetry including MnTe [36, 37], RuO_2 [38] and CrSb [39–41].

While it is true that none of the above altermagnets have been yet reported to show superconductivity, research in this area is still in very early stages and many more candidate altermagnet families have been identified by the recent theoretical work, both in naturally occurring crystals [42–47] and in artificially engineered structures [48]. Since many of these are good metals it would be surprising if at least some did not show superconducting instabilities when cooled down to low temperatures. It is also worth emphasizing that the predicted unconventional equal-spin pairing does not require any exotic pairing mechanism – it emerges naturally as the leading SC instability of the altermagnetic normal metal in the presence of conventional weak attraction mediated by phonons [34] or any other bosonic mode.

We remark that *proximity-induced* superconductivity in altermagnets has been studied by a number of authors [49–54]. Structures formed of conventional superconductors and altermagnets have been predicted to show a multitude of interesting and potentially useful behaviors including supercurrent-induced edge magnetization, Cooper pair spin-splitter and filtering effect, controllable $0 - \pi$ transitions in the Josephson supercurrent, spin-polarized Andreev levels and Josephson diode effect. The focus of this work, by contrast, is *intrinsic* SC order in altermagnets which remains relatively unexplored.

II. MICROSCOPIC MODELS

A. d -wave altermagnet

We consider a minimal model of a ‘ d -wave’ altermagnetic metal [19, 20] in two dimensions defined by the Hamiltonian $\mathcal{H}_0 = \sum_{\mathbf{k}} \psi_{\mathbf{k}}^\dagger h_0(\mathbf{k}) \psi_{\mathbf{k}}$ with $\psi_{\mathbf{k}} = (c_{\mathbf{k}\uparrow}, c_{\mathbf{k}\downarrow})^T$ and

$$h_0(\mathbf{k}) = -2t(\cos k_x + \cos k_y) - 2\eta\sigma_z(\cos k_x - \cos k_y). \quad (1)$$

Here σ_μ are Pauli matrices in spin space, t denotes the nearest neighbor hopping amplitude on the square lattice. The η term gives the altermagnetic band splitting and hence breaks time-reversal symmetry \mathcal{T} . The model however remains invariant under combined C_4 rotation and \mathcal{T} , a hallmark feature of altermagnets which guarantees vanishing total magnetization. Unlike conventional antiferromagnetism, altermagnetic order does not enlarge the non-magnetic unit cell. Thus, the crystallographic basis of altermagnets is, in principle, required to contain at least two sites. While interband effects have been

shown to be an important factor in the microscopic formation of altermagnetic order [55, 56], the corresponding Néel temperatures tend to be orders of magnitude larger than the superconducting energy scales considered here. Consequently, we can safely neglect coupling between different sublattices and consider an effective single-band model (1) with altermagnetic splitting introduced through spin-dependent tunneling amplitudes.

When the inversion symmetry of \mathcal{H}_0 is broken (e.g. by placing the system on a substrate) then a Rashba SOC term

$$h_R(\mathbf{k}) = 2\lambda_R(\sigma_x \sin k_y - \sigma_y \sin k_x) \quad (2)$$

becomes symmetry-allowed. The main effect of non-zero λ_R is to resolve the remaining Fermi surface degeneracies along the Brillouin zone diagonals visible in Fig. 1(a). In the vicinity of these points the Rashba term causes the spins to rotate into the plane.

B. g -wave altermagnet

Although a purely 2D model of a g -wave altermagnet can be defined [57], it requires a rather large unit cell which does not correspond to any known naturally occurring material. We therefore take inspiration from the crystal structure of CrSb, which is a confirmed altermagnetic metal [39, 40] and introduce an effective 3D model on a layered triangular lattice which produces a qualitatively correct spin-split Fermi surface. The Hamiltonian is given as

$$h_0(\mathbf{k}) = -2t \sum_j \cos \delta_j \cdot \mathbf{k} - 2t_z \cos k_z - 2\eta \sum_j \cos [\sigma_z k_z + (\delta_j - \delta_{j-1}) \cdot \mathbf{k}], \quad (3)$$

where $\delta_1 = \hat{x}$ and $\delta_{2,3} = -\frac{1}{2}(\hat{x} \mp \sqrt{3}\hat{y})$ are nearest neighbor vectors on the triangular lattice. t_z denotes the interlayer tunneling amplitude and the η term produces the characteristic g -wave altermagnetic spin splitting depicted in Fig. 1. This term breaks \mathcal{T} but the model remains invariant under combined C_{6z} rotation and \mathcal{T} which qualifies it as a g -wave altermagnet.

To account for the relativistic effects a Dresselhaus-type SOC of the form

$$h_D(\mathbf{k}) = 2\lambda_D \sum_{j,\alpha=\pm} \sigma^{(j)} \sin [\alpha k_z + (\delta_j - \delta_{j-1}) \cdot \mathbf{k}], \quad (4)$$

where $\sigma^{(j)} = \boldsymbol{\sigma} \cdot [\hat{z} \times (\delta_j - \delta_{j-1})]$, can be added. This term respects \mathcal{T} but is odd under inversion \mathcal{P} . Similar to h_R its chief effect is to split the remaining spin degeneracies located on high-symmetry planes that follow from the non-relativistic Hamiltonian Eq. (3). In addition, SOC terms Eq. (2) and (4) break the $U(1)_\uparrow \times U(1)_\downarrow$ symmetry associated with the separate number conservation of spin-up and spin-down electrons down to a single $U(1)$ charge conservation symmetry.

In the following, we will consider superconducting instabilities of \mathcal{H}_0 for both the d - and g -wave model altermagnets in the presence of weak attractive interaction. When specified we will study the effect of weak SOC with magnitude small compared to the SC gap, as well as magnetic disorder described by a Hamiltonian specified below. We will take $t = 1$ and express all energies in units of t .

C. Pairing instabilities

To study SC instabilities of the altermagnetic normal metals introduced above we consider Hamiltonian $\mathcal{H} = \mathcal{H}_0 + \mathcal{H}_I$ where

$$\mathcal{H}_0 = \sum_{\mathbf{k}} \psi_{\mathbf{k}}^\dagger [h_{\mathbf{k}} - \mu] \psi_{\mathbf{k}} \quad (5)$$

describes the underlying normal metal with $h_{\mathbf{k}}$ defined as a sum of $h_0(\mathbf{k})$ and the corresponding SOC terms given in Eqs. (1-4) above. For both d - and g -wave cases we consider in-plane nearest-neighbor attraction defined in real space as

$$\mathcal{H}_I = -V_1 \sum_{\langle i,j \rangle} n_i n_j \quad (6)$$

where V_1 is a positive interaction parameter and $n_j = \sum_{\sigma} c_{j\sigma}^\dagger c_{j\sigma}$ denotes the electron number operator on site j .

We next perform standard mean-field decoupling of \mathcal{H}_I in spin-singlet and equal-spin triplet channels and define the corresponding SC order parameters

$$\Delta_{ij}^0 = V_1 \langle c_{i\uparrow} c_{j\downarrow} \rangle, \quad \Delta_{ij}^\sigma = V_1 \langle c_{i\sigma} c_{j\sigma} \rangle, \quad (7)$$

associated with a bond between nearest neighbor sites i and j . The singlet component is even under inversion, $\Delta_{ij}^0 = \Delta_{ji}^0$, and can be thought of as an extended s -wave order parameter. The triplet component must be inversion-odd, $\Delta_{ij}^\sigma = -\Delta_{ji}^\sigma$, and can be realized as a p -wave order parameter.

Our discussion thus far has been completely general in that it applies to both d - and g -wave altermagnets and, after recasting h_0 in real space, the formalism can describe spatially non-uniform situations such as in the presence of boundaries or currents. We now wish to study the competition between singlet and triplet instabilities. To this end we specialize to spatially uniform configurations of the order parameters by assuming

$$\Delta_{ij}^0 = \Delta_0, \quad \Delta_{ij}^\sigma = e^{\pm i\theta_{ij}} \Delta_\sigma, \quad (8)$$

where θ_{ij} denotes the angle between the bond and the positive x axis. Δ_{ij}^σ in Eq. (8) describes the chiral p -wave order parameter (with \pm sign reflecting the two possible chiralities). We expect such chiral $p_x \pm ip_y$ order parameter to be energetically favored over pure p_x or p_y

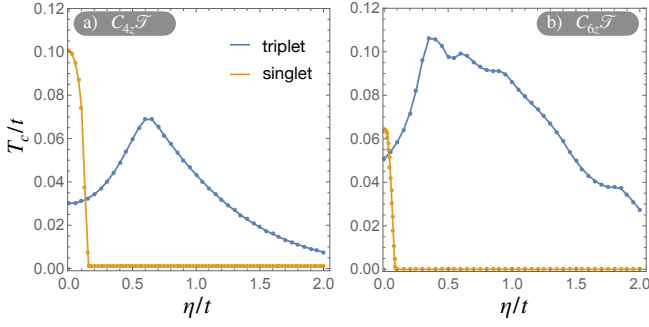


FIG. 2. Superconducting critical temperatures in singlet and triplet channels extracted from numerical solutions to gap equations (13a) and (13b) for (a) d -wave and (b) g -wave model altermagnetic metals. We use $(\mu, V_1) = (-2.6, 1.93)t$ for d -wave and $(-2.0, 1.95)t$ for g -wave as representative parameters.

because it generally leads to a fully gapped fermi surface. In the language of Ref. [29] these phases belong among the family “spin chiral” superconductors.

In momentum space the decoupled interaction Hamiltonians take the following form

$$\mathcal{H}_{\text{MF}}^0 = 2\Delta_0 \sum_{\mathbf{k}} C_{\mathbf{k}} (c_{\mathbf{k}\uparrow}^\dagger c_{-\mathbf{k}\downarrow}^\dagger + \text{h.c.}) + \frac{4N}{V_1} \Delta_0^2, \quad (9a)$$

$$\mathcal{H}_{\text{MF}}^\sigma = \Delta_\sigma \sum_{\mathbf{k}} (S_{\mathbf{k}\sigma} c_{\mathbf{k}\sigma}^\dagger c_{-\mathbf{k}\sigma}^\dagger + \text{h.c.}) + \frac{2N}{V_1} \Delta_\sigma^2, \quad (9b)$$

where on the square lattice

$$C_{\mathbf{k}} = \cos k_x + \cos k_y, \quad S_{\mathbf{k}\sigma} = \sin k_x \pm i \sin k_y, \quad (10)$$

and analogous expressions for the triangular lattice. This leads to a description in terms of the Bogoliubov-de Gennes (BdG) Hamiltonian

$$\mathcal{H}_{\text{BdG}} = \sum_{\mathbf{k}} \Psi_{\mathbf{k}}^\dagger \begin{pmatrix} h_{\mathbf{k}} - \mu & \hat{\Delta}_{\mathbf{k}} \\ \hat{\Delta}_{\mathbf{k}}^\dagger & -h_{-\mathbf{k}}^* + \mu \end{pmatrix} \Psi_{\mathbf{k}} + E_0, \quad (11)$$

where $\Psi_{\mathbf{k}} = (c_{\mathbf{k}\uparrow}, c_{\mathbf{k}\downarrow}, c_{-\mathbf{k}\uparrow}^\dagger, c_{-\mathbf{k}\downarrow}^\dagger)^T$ is the Nambu spinor,

$$\hat{\Delta}_{\mathbf{k}} = \begin{pmatrix} \Delta_\uparrow S_{\mathbf{k}\uparrow} & \Delta_0 C_{\mathbf{k}} \\ -\Delta_0 C_{\mathbf{k}} & \Delta_\downarrow S_{\mathbf{k}\downarrow} \end{pmatrix}, \quad (12)$$

and $E_0 = \sum_{\mathbf{k}} \text{Tr}(h_{\mathbf{k}}) + \frac{2N}{V_1} (2\Delta_0^2 + \Delta_\uparrow^2 + \Delta_\downarrow^2)$.

To study the competition between singlet and triplet channels we now focus on the non-relativistic case where SOC terms are absent. The system then respects the inversion symmetry and the two order parameters belong to different irreducible representations of the point group. In this situation, when only one order parameter is non-zero, the 4×4 BdG matrix in Eq. (11) can be recast as a 2×2 matrix in the relevant subspace and can be easily diagonalized. The corresponding BdG energy eigenvalues are found as

$$E_{\mathbf{k}0} = \xi_{\mathbf{k}-} \pm \sqrt{\xi_{\mathbf{k}+}^2 + \Delta_0^2 C_{\mathbf{k}}^2}, \quad (\text{singlet}) \quad (13a)$$

$$E_{\mathbf{k}\sigma} = \pm \sqrt{\xi_{\mathbf{k}\sigma}^2 + \Delta_\sigma^2 |S_{\mathbf{k}\sigma}|^2}. \quad (\text{triplet}) \quad (13b)$$

Here $\xi_{\mathbf{k}\sigma}$ are the eigenvalues of $h_0(\mathbf{k})$ referenced to the chemical potential μ and $\xi_{\mathbf{k}\pm} = (\xi_{\mathbf{k}\uparrow} \pm \xi_{\mathbf{k}\downarrow})/2$.

From the knowledge of the energy eigenvalues it is straightforward to construct the free energy F of the system and obtain the corresponding gap parameters by minimizing F with respect to the order parameters. We thus find

$$\Delta_0 = \frac{V_1}{2N} \sum_{\mathbf{k}} \frac{\Delta_0 C_{\mathbf{k}}^2}{\epsilon_{\mathbf{k}}} \frac{\sinh \beta \epsilon_{\mathbf{k}}}{\cosh \beta \xi_{\mathbf{k}-} + \cosh \beta \epsilon_{\mathbf{k}}}, \quad (14a)$$

$$\Delta_\sigma = \frac{V_1}{2N} \sum_{\mathbf{k}} \frac{\Delta_\sigma |S_{\mathbf{k}\sigma}|^2}{E_{\mathbf{k}\sigma}} \tanh \frac{1}{2} \beta E_{\mathbf{k}\sigma}, \quad (14b)$$

where $\epsilon_{\mathbf{k}} = \sqrt{\xi_{\mathbf{k}+}^2 + \Delta_0^2 C_{\mathbf{k}}^2}$ and $\beta = 1/k_B T$ denotes the inverse temperature. We observe that while the gap equation for the triplet order parameter (14b) assumes the standard BCS form, Eq. (14a) is non-standard in that it shows explicit dependence on the altermagnetic spin splitting through $\xi_{\mathbf{k}-} \sim \eta$. This reflects the expectation that spin-singlet pairing will be sensitive to the \mathcal{T} breaking present in the altermagnet while triplet pairing will not.

We solve Eqs. (13a) and (13b) numerically and show the behavior of superconducting critical temperatures for singlet s -wave and triplet $p_x \pm ip_y$ order parameters as a function of spin splitting η in Fig. 2. The behavior supports the general argument made in Sec. I. As expected, the leading SC instability for a spin-degenerate Fermi surface at $\eta = 0$ occurs in the singlet channel which is signaled by higher singlet T_c . However, even small values of η cause rapid suppression of the singlet T_c – altermagnetic spin splitting is strongly pair breaking for singlet Cooper pairs. By contrast the triplet T_c is largely unaffected and even grows with increasing η . (This initial rise of T_c is attributed to the increase with η of the Fermi surface size and hence the density of states N_F . At a constant interaction strength V_1 the standard BCS expression $T_c \propto e^{-1/N_F V_1}$ then implies increasing T_c .)

Crucially, when $\eta \gtrsim \Delta_0$ the equal-spin triplet $p_x \pm ip_y$ channel becomes the leading SC instability. In altermagnetic metals η is typically of the order of hundreds of meV and can be as large as ~ 1 eV. Typical values of Δ_0 will be 1 – 10 meV. This leads to a firm conclusion that superconductivity in any altermagnet will almost certainly be in the equal-spin triplet channel.

For the sake of completeness we also investigated the gap equation for the p_x and p_y case, which assume the same form as Eq. (14b) with $S_{\mathbf{k}} = \sin k_{x/y}$. The corresponding T_c is more than an order of magnitude smaller compared to the chiral $p_x \pm ip_y$ case for the range of model parameters that we investigated. Hence, these p -wave channels are not competitive.

We note, finally, that the behavior depicted in Fig. 2 is quite generic, in that spin-singlet order parameter is always strongly suppressed by altermagnetic splitting whereas spin-triplet is not. The detailed dependence of critical temperatures is sensitive to the model details but

TABLE I. Four degenerate ground states of the equal-spin triplet chiral p -wave superconductor in the non-relativistic limit.

| Ground state | Abbreviation | Chern number | Property |
|---|---------------------------------------|--------------|----------|
| $ \uparrow\uparrow(p_x + ip_y)\rangle \otimes \downarrow\downarrow(p_x + ip_y)\rangle$ | $p_+^\uparrow \otimes p_+^\downarrow$ | +2 | chiral |
| $ \uparrow\uparrow(p_x - ip_y)\rangle \otimes \downarrow\downarrow(p_x + ip_y)\rangle$ | $p_+^\uparrow \otimes p_+^\downarrow$ | 0 | helical |
| $ \uparrow\uparrow(p_x + ip_y)\rangle \otimes \downarrow\downarrow(p_x - ip_y)\rangle$ | $p_+^\uparrow \otimes p_-^\downarrow$ | 0 | helical |
| $ \uparrow\uparrow(p_x - ip_y)\rangle \otimes \downarrow\downarrow(p_x - ip_y)\rangle$ | $p_-^\uparrow \otimes p_-^\downarrow$ | -2 | chiral |

the above basic feature is a robust property of altermagnetic metals. One can, for instance, add an on-site attraction V_0 to \mathcal{H}_I defined in Eq. (6). This has the effect of boosting T_c of the singlet channel for small η . Nevertheless, the singlet T_c is still strongly suppressed by spin splitting and the triplet order robustly prevails when $\eta > \Delta_0$.

In the rest of this paper we focus on the limit of moderate to large spin splitting parameter η where the ground state is equal-spin triplet chiral p -wave superconductor. In the non-relativistic limit such a ground state exhibits a four-fold degeneracy due to two possible chiralities for each spin. Two of the ground states are helical and two are chiral as listed in Table 1. The assignment of the Chern number follows from the fact that a spinless $p_x \pm ip_y$ state has Chern number $C = \pm 1$, respectively [58]. Correspondingly, when placed on a geometry with open edges, such as a long strip, the 4 ground states will show protected edge modes that are either chiral for $C = \pm 2$ states, or helical for $C = 0$ states. Because the chiral edge modes carry substantial electrical currents [59], one expects, for small samples, the helical states to be lower in energy when one includes the inductive effects, that is, the energy cost of the magnetic field B produced by the edge current. As we shall see helical edge states carry an aggregate spin current which however produces no magnetic field; hence, we expect helical states to be lower in energy than chiral states even in the strictly non-relativistic limit.

In the presence of various perturbations the ground state degeneracy will be lifted even in large samples. For the $C_{2z}\mathcal{T}$ model this has been investigated in Refs. [30, 32]. According to these works Rashba SOC selects helical $p_+^\uparrow \otimes p_+^\downarrow$ as the unique ground state. In-plane magnetic field on the other hand selects the two chiral states which remain degenerate. For the sake of concreteness we will in the following assume weak SOC and focus on the helical $p_+^\uparrow \otimes p_+^\downarrow$ state in our calculations. However, we note that a majority of the results pertaining to spin currents presented in the rest of this paper are insensitive to the choice of the ground state.

III. SPIN-POLARIZED SUPERCURRENT GENERATION IN d -WAVE ALTERMAGNETS

A. General considerations

As our first example of useful spintronic properties of SC altermagnets we show that they can be used to generate persistent spin currents. This property is most pronounced in d -wave altermagnets with equal-spin triplet superconducting order and relies on the fact that the underlying fermi surfaces possess low C_{2z} symmetry for each spin projection, cf. Fig. 1(a). In this situation it is easy to see that the superfluid density tensor $\hat{\rho}_\sigma$, which governs the supercurrent response of the material according to

$$\mathbf{j}_\sigma = \hat{\rho}_\sigma \left(\hbar \nabla \varphi_\sigma - \frac{2e}{c} \mathbf{A} \right), \quad (15)$$

will be anisotropic with *opposite* anisotropies for the two spin projections. Here \mathbf{j}_σ is the supercurrent density carried by condensate Δ_σ and φ_σ is its phase. Because Cooper pairs with either spin carry the same charge $2e$ they couple identically to the vector potential \mathbf{A} . However, phases φ_σ can in general be different.

The C_{2z} symmetry of the band dispersion for each spin constrains the form of $\hat{\rho}_\sigma$ such that

$$\hat{\rho}_\sigma = \begin{pmatrix} \rho_0 & 0 \\ 0 & \rho_0 \end{pmatrix} + \sigma \begin{pmatrix} \rho_\eta & 0 \\ 0 & -\rho_\eta \end{pmatrix}, \quad (16)$$

where ρ_0 denotes the conventional isotropic component and ρ_η is the anisotropy related to the altermagnetic spin splitting, which is, crucially, opposite for two spin projections labeled by $\sigma = \pm$. The form of the superfluid density tensor Eq. (16) is clearly compatible with the $C_{4z}\mathcal{T}$ symmetry of a d -wave altermagnet. Microscopically it follows from the fact that the superfluid density tensor is proportional to the inverse effective mass tensor, $[\hat{\rho}_\sigma]_{\alpha\beta} \propto \partial^2 \epsilon_{\mathbf{k}\sigma} / \partial k_\alpha \partial k_\beta |_{\mathbf{k}=0}$. For completeness we review the relevant arguments in Appendix A where we also find, for the d -wave altermagnet model defined in Section II,

$$\rho_0 \simeq n_e, \quad \rho_\eta \simeq (\eta/t)n_e, \quad (17)$$

where n_e denotes the electron density.

To explore the consequences of Eq. (16) let us first assume, for the sake of simplicity, that the two condensates experience the same superfluid velocities $\mathbf{v}_\sigma =$

$(\hbar\nabla\varphi_\sigma - \frac{2e}{c}\mathbf{A})$. This occurs e.g. when the current is driven principally by \mathbf{A} or when the phases φ_\uparrow and φ_\downarrow are locked together energetically by SOC. (We will explore the effects of unequal velocities in later Sections.) In this situation it is easy to deduce from Eqs. (15) and (16) that the electrical current $\mathbf{j}^e = \mathbf{j}_\uparrow + \mathbf{j}_\downarrow$ will be governed by ρ_0 while the spin current $\mathbf{j}^s = \mathbf{j}_\uparrow - \mathbf{j}_\downarrow$ by ρ_η , namely

$$\mathbf{j}^e = \rho_0 \mathbf{v}, \quad \mathbf{j}^s = \rho_\eta \tau^z \mathbf{v}. \quad (18)$$

Here \mathbf{v} is the common superfluid velocity of the two condensates and τ^z is the third Pauli matrix. From Eq. (18) one can also express the spin current in terms of the electrical current as

$$\mathbf{j}^s = (\rho_\eta/\rho_0) \tau^z \mathbf{j}^e. \quad (19)$$

The simple-looking equation (19) has some interesting consequences illustrated in Fig. 3(a). It implies that a persistent electrical current \mathbf{j}^e directed along x or y principal axes will be accompanied by a persistent spin current $\mathbf{j}^s = (\rho_\eta/\rho_0) \mathbf{j}^e$ along the same direction. Even more remarkably, when \mathbf{j}^e is directed along the diagonal, e.g. (1,1) direction, spin current will flow along the orthogonal (1,-1) direction. As depicted in Fig. 3(b) this property can be exploited to generate pure spin supercurrent with the magnitude controllable by the applied charge current in the transverse direction. This pure spin supercurrent then can be injected from the SC altermagnet into another material; we call this *spin-current dynamo* effect and explore it in more detail below. It can be thought of as a superconducting version of the electrical spin splitter effect discussed in the context of organic antiferromagnets and RuO₂ in Refs. [42] and [60], respectively. More broadly, the spin-current dynamo effect belongs to the family of spin Hall effects that play an important role in the field of spintronics [4].

B. Spin current dynamo effect

To confirm the validity of general arguments given in the previous subsection we now perform numerical calculations using the BdG Hamiltonian Eq. (11) formulated on the real-space square lattice. We carry out two types of calculations addressing different geometries. Specifically, we diagonalize the real-space Hamiltonian for (i) a spatially uniform order parameter Δ_σ on an $L \times L$ cluster with periodic boundary conditions and (ii) on a $L_x \times L_y$ strip in the “dynamo” geometry Fig. 3(b) with periodic boundary conditions along x and current injected through 10 sites at the bottom open edge and extracted through top sites. In both cases we probe currents by computing expectation values of the spin-resolved bond current operator

$$j_{ij}^\sigma = -it_{ij}^\sigma c_j^\dagger c_{i\sigma} + \text{h.c.} \quad (20)$$

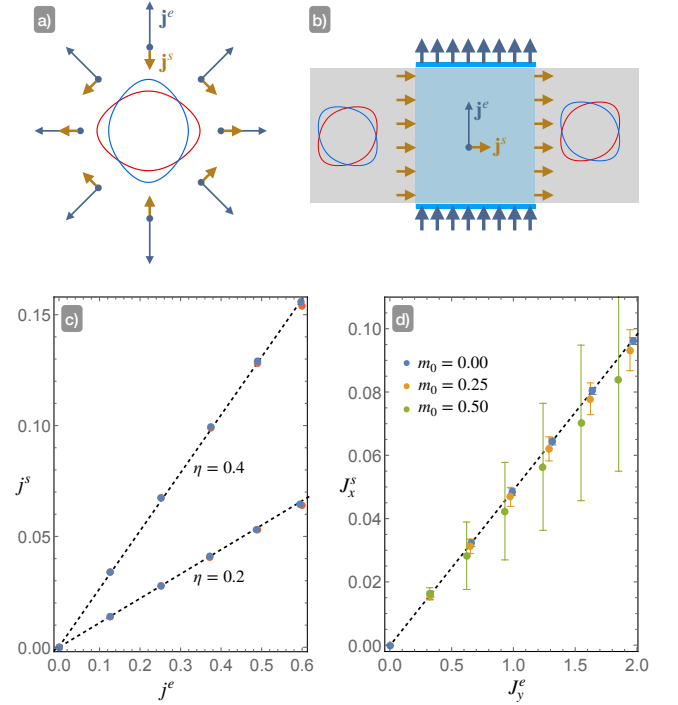


FIG. 3. Spin-polarized supercurrent generation in a d -wave altermagnet. Panel (a) visualizes the relation between \mathbf{j}^s and \mathbf{j}^e expressed by Eq. (19). Panel (b) illustrates the spin-current dynamo effect which may be used to generate pure spin supercurrent by applying ordinary charge current to a strip oriented along the (1,1) direction relative to the underlying altermagnet principal axes. In (c) we show spin current density j^s as a function of j^e (both in the units of t) for a 20×20 cluster with periodic boundary conditions. Blue (orange) symbols correspond to \mathbf{j}^e flowing along \hat{x} ($\hat{x} + \hat{y}$) direction. Panel (d) shows spin current J_x^s as a function of J_y^e in the dynamo geometry for the system studied in Fig. 4. Data points represent the total spin current averaged over 40 positions along \hat{x} while the error bar quantifies its fluctuation computed as a standard deviation of these values. Parameters used are $\mu = -2.1$, $V_1 = 2.0$ with $\eta = 0.2$ in panel (d).

where t_{ij}^σ denotes the tunneling amplitude between sites i and j for electrons with spin σ .

Case (i) geometry corresponds to a torus and we drive electrical current \mathbf{j}^e by inserting magnetic fluxes Φ_x and Φ_y through the two holes of the torus. This is implemented through a Peierls substitution $t_{ij}^\sigma \rightarrow t_{ij}^\sigma \exp[-i(\mathbf{r}_i - \mathbf{r}_j) \cdot \mathbf{A}]$ where $\mathbf{A} = \pi(\Phi_x, \Phi_y)/L\Phi_0$ is the vector potential. By adjusting the fluxes we can drive charge current \mathbf{j}^e in any desirable direction. Subsequent measurements of \mathbf{j}^s are summarized in Fig. 3(c) and give results that are in a good qualitative agreement with the prediction of Eq. (19). The relation between j^s and j^e is indeed linear with the coefficient proportional to η/t and about factor of 2 smaller than the estimate based on the quadratic dispersion.

Fig. 4 shows our results for the dynamo geometry case (ii) in a cluster of 40×10 sites. In order to accommodate

this geometry naturally on a square lattice we modify the normal state Hamiltonian by rotating the spin-dependent term in Eq. (1) by 45° which gives

$$-2\eta\sigma_z[\cos(k_x + k_y) - \cos(k_x - k_y)]. \quad (21)$$

This produces a d_{xy} altermagnet with fermi surface crossings along x and y axes and allows us to straightforwardly implement the geometry indicated in Fig. 3(b). To probe the dynamo effect we then drive charge current in the vertical direction through the central portion of the strip. This is achieved by connecting sites at the bottom edge of the strip with their partners at the same position x at the top edge through a spin-independent hopping amplitude $t_J e^{-i\pi\Phi_x/\Phi_0}$. This creates a Josephson junction between a portion of the bottom and top edge biased by flux Φ_x . When Φ_x is non-zero current flows through the strip as indicated in Fig. 4(a,b) which shows the corresponding spin-resolved current densities. We remark that in this constrained geometry it is important to use self-consistently determined order parameter amplitudes (shown as colorscale background) in order to ensure current conservation.

Panel (c) displays current densities resolved into their charge and spin components indicated by blue and orange arrows, respectively. The spin current density is dominated by prominent edge contributions flowing along the open edges of the strip. These are indeed expected due to the presence of topologically protected edge modes in the $p_-^\uparrow \otimes p_+^\downarrow$ superconductor which are known to carry substantial currents [59]. Because of their spin-filtered helical nature the corresponding charge current density vanishes but significant spin current is seen to remain. The modes are however exactly counterbalanced between the two edges and carry therefore no net spin (or charge) current along the strip. In order to visualize the spin-current dynamo effect we display in panel (d) spin current density referenced to the situation with $\Phi_x = 0$ where no charge current is driven across the strip. This subtraction eliminates the edge currents and allows us to clearly see that bulk spin current is flowing along the strip.

In order to ascertain the robustness of the spin current dynamo effect we now consider the effect of magnetic disorder. To this end we include a term

$$\mathcal{H}_{\text{dis}} = \sum_j \mathbf{m}_j \cdot \boldsymbol{\sigma}_{\alpha\beta} c_{j\alpha}^\dagger c_{j\beta} \quad (22)$$

in the normal-state electron Hamiltonian where \mathbf{m}_j represents a static local magnetic moment on site j . We take Cartesian components of \mathbf{m}_j as random independent variables drawn from a uniform distribution between $(-m_0, m_0)$. This corresponds to a random magnetic moment with mean-square amplitude $\langle \mathbf{m}_j^2 \rangle^{1/2} = m_0$ on every site of the lattice coupled to electron spin. Panels (e-h) of Fig. 4 show the effect of moderately strong disorder $m_0 = 0.25t$ which corresponds to about half of the SC gap amplitude Δ_σ . We observe clear effects of disorder in local fluctuations of the gap amplitude, although

its average value is only mildly suppressed. The current flow is also affected and shows visible local fluctuations in current densities when compared to the clean case.

It is to be noted that spin current is no longer conserved in the presence of \mathcal{H}_{dis} because non-zero in-plane components of \mathbf{m}_j generate spin-flip scattering. Nevertheless we observe in panel (h) a clear evidence of the dynamo effect with a magnitude that is comparable to the clean case. This is quantified in panel (d) of Fig. 3, where we show the total spin current J_x^s flowing along the strip in response to charge current J_y^e for three representative disorder strengths m_0 . Because of the non-conservation mentioned above J_x^s fluctuates as a function of position x along the strip when $m_0 \neq 0$. To provide a sense for these fluctuations we display in Fig. 3(d) both the average value of J_x^s and its standard deviation. We observe that fluctuations are modest for $m_0 = 0.25$ but become large for $m_0 = 0.50$, even though the average value is suppressed only slightly. We remark that $m_0 = 0.50$ corresponds to the limit of very strong disorder with the magnetic impurity strength on each site exceeding the size of the SC gap $\Delta_\sigma \simeq 0.42$. It is remarkable that the spin current dynamo effect survives essentially intact even in this highly disordered limit.

Some remarks are in order before we conclude this Section. First, we note that the $C_{6z}\mathcal{T}$ symmetry of g -wave altermagnets mandates that $\rho_\eta = 0$ and hence they cannot be used to generate spin currents in this fashion; however, the effect might reemerge when strain is applied [61]. Interesting properties besides spin current generation are explored below. Second, our general analysis leading to Eq. (19) relied crucially on the simplifying assumption of equal superfluid velocities \mathbf{v}_σ for the two spin species. In reality the two phases φ_σ are independent degrees of freedom that assume spatial profiles so as to minimize the system free energy under the specific conditions imposed by the experimental setup. Hence, generically, \mathbf{v}_\uparrow need not equal \mathbf{v}_\downarrow . Nevertheless for the geometries considered in this Section we found Eq. (19) to be in a good agreement with the numerical simulations in which φ_σ are treated as independent variables and are computed selfconsistently from the gap equation.

Finally, we note that the spin current generated by the dynamo effect is odd under $\eta \rightarrow -\eta$. This implies that if multiple magnetic domains are present in the sample their contributions to j^s will tend to average out. To achieve a significant effect one thus ideally requires a single-domain sample or a sample dominated by one magnetic domain. In the recent experiment on altermagnet MnTe domain sizes greater than $10\mu\text{m}$ have been reported with careful annealing [62].

IV. PERSISTENT SPIN CURRENT IN VARIOUS GEOMETRIES

A key conclusion reached in Section II was that the leading SC instability in an altermagnet with large

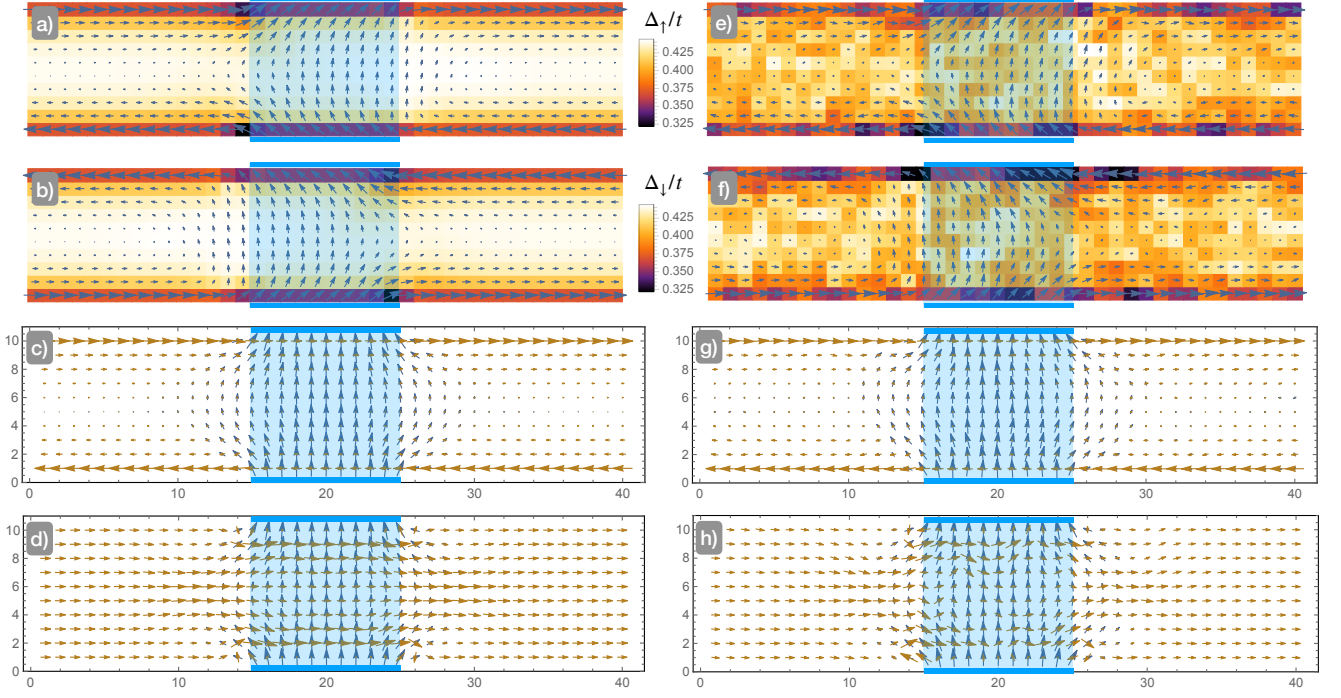


FIG. 4. Spin-current dynamo effect: Generation of pure spin supercurrent from perpendicular charge current. Panels (a) and (b) show current densities \mathbf{j}_\uparrow and \mathbf{j}_\downarrow calculated from the BdG theory for a 40×10 cluster of sites with periodic boundary conditions along x . The current is injected through the bottom blue electrode and collected from the top blue electrode. The colorscale indicates the amplitude of the self-consistently determined SC order parameter Δ_σ . Panel (c) shows the current densities resolved into the electrical component \mathbf{j}^e and spin component \mathbf{j}^s , represented by blue and orange arrows, respectively. Panel (d) shows those same currents relative to the reference state when no external current is injected. Panels (e-h) show the same quantities for the system with magnetic disorder with $m_0 = 0.25t$. Spin currents in panels (d,h) have been scaled up by a factor of 6 for better visibility. Parameters are the same as in Fig. 3 with $t_J = 1.0$ and $\Phi_x = 0.4\Phi_0$.

enough spin splitting η occurs in the equal-spin triplet channel. In the absence of SOC this leads to two decoupled condensates, one for spin-up and one for spin-down electrons represented by Δ_\uparrow and Δ_\downarrow order parameters. At a high level it is intuitively clear that such decoupled condensates are capable of supporting persistent currents with an arbitrary spin polarization, including pure spin supercurrent $\mathbf{j}^s \neq 0$ with $\mathbf{j}^e = 0$, achieved when spin-up charge current \mathbf{j}_\uparrow is exactly counterbalanced by an opposite \mathbf{j}_\downarrow .

To better understand various properties of these persistent currents in different situations and also to understand the effect of SOC we now construct the Ginzburg-Landau (GL) theory for the equal-spin triplet superconductor and analyze its solutions in various relevant geometries.

A. Ginzburg-Landau theory

The GL free energy density for the equal-spin triplet superconductor can be written as

$$f[\psi_\uparrow, \psi_\downarrow] = \sum_\sigma f_\sigma[\psi_\sigma] - \frac{1}{2}D(\psi_\uparrow^* \psi_\downarrow + \text{c.c.}) + \frac{B^2}{8\pi}, \quad (23)$$

where ψ_σ are complex scalar order parameters describing the two condensates and f_σ is the standard GL free energy density for the individual condensate,

$$f_\sigma[\psi] = \alpha|\psi|^2 + \frac{1}{2}\beta|\psi|^4 + \gamma_\sigma|i\nabla + \frac{2e}{\hbar c}\mathbf{A}\psi|^2. \quad (24)$$

By symmetry the α and β parameters must be the same for the two condensates. For a d -wave altermagnet the γ parameter becomes a tensor which reflects the superfluid density anisotropy discussed in Sec. III. In the following, for the sake of maximum clarity and simplicity, we focus on the isotropic case where γ_σ is taken as a constant equal to γ for both condensates. Such theory is directly applicable to g -wave altermagnets and can also describe multidomain d -wave altermagnets on long lengthscales where the anisotropy has averaged out.

The D term in Eq. (23) describes coupling between the two condensates and becomes symmetry-allowed in the presence of SOC for the two helical states listed in Table 1. In this situation we expect $D \propto \lambda^2$ where λ stands for either Rashba λ_R in 2D or Dresselhaus λ_D in 3D. We note that for the two chiral states the D term is not allowed. As explained in Appendix B in this case the leading allowed coupling is a fourth-order term ($\psi_\uparrow^{2*} \psi_\downarrow^2 + \text{c.c.}$) and has a prefactor proportional to λ^4 .

Since we are mostly interested in the behavior of persistent currents on long distances compared to the SC coherence length ξ we adopt the London approximation $\psi_\sigma = \psi_0 e^{i\varphi_\sigma}$ with spatially constant ψ_0 , whose value we take as real and positive. This leads to a Josephson free energy density of the form

$$f[\varphi_\uparrow, \varphi_\downarrow] = f_0 + \sum_\sigma \gamma \psi_0^2 (\nabla \varphi_\sigma - \frac{2e}{\hbar c} \mathbf{A})^2 - J \cos(\varphi_\uparrow - \varphi_\downarrow) \quad (25)$$

where f_0 is the component independent of the phases (which we suppress from now on) and $J = \psi_0^2 D$. The last term expresses the energy cost for configurations where two phases are not aligned and can therefore be thought of as describing an internal Josephson effect. A direct calculation of J from the microscopic d -wave model is outlined in Appendix B and gives

$$J \simeq \lambda_R^2 k_F^4 / 4\pi t, \quad (26)$$

where $k_F = \sqrt{(\mu + 4t)/t}$ is the dimensionless Fermi momentum. Eq. (26) assumes the $p_-^\uparrow \otimes p_+^\downarrow$ helical phase and is valid for $\lambda_R \lesssim \Delta_\sigma$ and μ near the bottom of the band, that is, $k_F \lesssim 1$.

It is convenient for our subsequent considerations to define average and relative phases

$$\Omega = \frac{1}{2}(\varphi_\uparrow + \varphi_\downarrow), \quad \varphi = \varphi_\uparrow - \varphi_\downarrow$$

and rewrite Eq. (25) as

$$f[\Omega, \varphi] = \gamma \psi_0^2 \left[2(\nabla \Omega - \frac{2e}{\hbar c} \mathbf{A})^2 + \frac{1}{2}(\nabla \varphi)^2 \right] - J \cos \varphi. \quad (27)$$

Charge current density then follows from varying the free energy $F = \int f dV$ with respect to \mathbf{A} , which gives

$$\mathbf{j}^e = \mathbf{j}_\uparrow + \mathbf{j}_\downarrow = 8e \frac{\gamma \psi_0^2}{\hbar} (\nabla \Omega - \frac{2e}{\hbar c} \mathbf{A}). \quad (28)$$

Similarly, we define the spin current density as

$$\mathbf{j}^s = \mathbf{j}_\uparrow - \mathbf{j}_\downarrow = 4e \frac{\gamma \psi_0^2}{\hbar} \nabla \varphi. \quad (29)$$

GL equations of motion follow from varying F with respect to the two phases. $\delta F / \delta \Omega = 0$ gives $\nabla \cdot \mathbf{j}^e = 0$ expressing the electrical current conservation. $\delta F / \delta \varphi = 0$ yields an equation of motion

$$\gamma \psi_0^2 \nabla^2 \varphi + J \sin \varphi = 0, \quad (30)$$

which must be solved subject to the appropriate boundary conditions in order to find the spin current. Below we discuss some specific examples.

B. Spin-polarized supercurrent in a long wire

A question of practical interest for any spintronic application is this: If we inject spin-polarized current into

a wire made of a SC altermagnet, how far from the injection point will the spin polarization persist? In the following we address this question by studying the GL theory derived above for a long wire geometry with the spin-polarized current injected from the left. We assume a homogeneous wire with the current injected at $x = 0$ flowing along the positive x direction. We consider a charge current with an arbitrary spin polarization expressed by specifying values of j^e and j^s .

We first consider the non-relativistic limit. In this case there is no SOC which translates to $J = 0$. Eq. (30) can then be recast as $\nabla \cdot \mathbf{j}^s = 0$ expressing spin current conservation exactly as one would expect when the two condensates are decoupled. Physically, this implies that *any* spin-polarization present in the injected current will persist to arbitrarily long lengthscales.

Away from the non-relativistic limit we have to include the effect of non-vanishing J . Qualitatively, it is clear from Eq. (29) that nonzero spin current requires nonzero gradient of the relative phase φ . This also means that φ cannot be uniformly zero to minimize the $-J \cos \varphi$ term in the free energy Eq. (27): the spin current will incur an energy cost. To see how this impacts the spin current amplitude along the wire we recast Eq. (30) as

$$\frac{d^2 \varphi}{dx^2} + k_J^2 \sin \varphi = 0, \quad (31)$$

where $k_J = \sqrt{J/\gamma \psi_0^2}$ is a constant with the dimension of inverse length. This is a second-order differential equation which we want to solve subject to boundary conditions at $x = 0$ for φ and its first derivative φ' . The latter is determined by the amplitude of the injected spin current through Eq. (29) while $\varphi_0 = \varphi(x = 0)$ can be fixed by physical conditions at the boundary, e.g. when the current is injected from another superconductor.

To gain some intuition for the solutions of Eq. (31), it is useful to note that it is mathematically equivalent to the equation of motion for the angle of a mechanical pendulum,

$$\frac{d^2 \varphi}{dt^2} + \omega^2 \sin \varphi = 0, \quad (32)$$

where $\omega = \sqrt{g/l}$ is the frequency of small oscillations. (g and l are the gravitational constant and the pendulum length, respectively.) Based on this analogy an important observation can be made right away. Because Eq. (31) corresponds to an *undamped* pendulum motion, we may conclude immediately that the spin current injected into the wire will not decay; instead, it will exhibit oscillations as a function of x with a constant amplitude. In analogy with the frictionless mechanical pendulum one expects two regimes for these oscillations: (i) the current can oscillate around zero which is analogous to small oscillations of the pendulum about the stable equilibrium at $\varphi = 0$, or (ii) it can oscillate around a non-zero value j_{avg}^s which corresponds to the pendulum rotating around the pivot with a steadily increasing angle. The two regimes

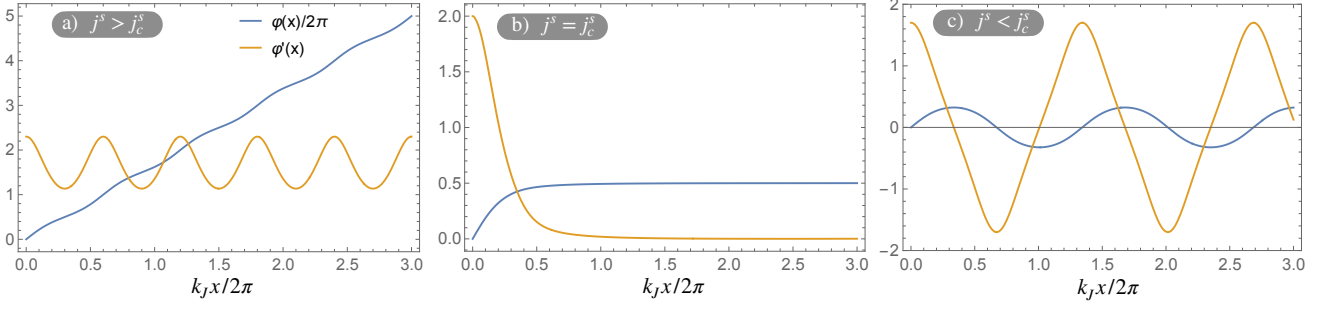


FIG. 5. Evolution of a spin current $j^s(x) \propto \varphi'(x)$ injected into a long wire at $x = 0$ in the presence of SOC. The current is obtained by numerically solving Eq. (31) with a boundary condition $\varphi(0) = 0$ and $\varphi'(0) = (2.3, 2.0, 1.7)k_J$ in panels (a), (b) and (c), respectively.

are separated by a critical point where the pendulum has just enough energy to reach the unstable equilibrium at the top of its trajectory.

Solutions of Eq. (31) displayed in Fig. 5 indeed confirm these expectations. When large enough spin current $j^s > j_c^s$ is injected panel (a) shows amplitude oscillations about a non-zero average value j_{avg}^s which persist without any decay to arbitrary distances. When smaller current $j^s < j_c^s$ is injected then the amplitude still oscillates without any decay but now around zero, panel (c). Only when the injected current is exactly tuned to the critical value $j^s = j_c^s$ it decays, panel (b). We note, however, that because this is an unstable fixed point (corresponding to a precisely tuned total energy in the pendulum analogy) an oscillatory behavior of one or the other type will generically occur. We conclude that even in the presence of SOC spin-polarized current injected into the wire will propagate to arbitrary distances without any decay. For $j^s < j_c^s$ one must detect it away from the nodes of the oscillatory profile depicted in Fig. 5(c) whereas for $j^s > j_c^s$ it can be detected everywhere along x .

To connect with experiment it is useful to estimate the period of spin-current oscillations and the critical spin current j_c^s which separates the two regimes. The period, given by $2\pi/k_J$, follows from recalling the well-known GL relations [63] for $\psi_0^2 = -\alpha/\beta$, the coherence length $\xi^2 = \gamma/|\alpha|^2$ and condensation energy $\frac{1}{2}N_F\Delta_0^2 = \alpha^2/2\beta$, where $N_F \simeq 1/4\pi t$ is the density of states at the Fermi level. Combining these with Eq. (26) one obtains

$$\frac{2\pi}{k_J} \simeq 2\pi\xi \left(\frac{\Delta_0}{\lambda_R} \right) k_F^{-2}, \quad (33)$$

valid when $\lambda_R \lesssim \Delta_0$. We observe that the period diverges when $\lambda_R \rightarrow 0$ and $\mu \rightarrow -4t$, in accord with expectations: in these limits coupling J between the two condensates vanishes. Even away from these extreme limits Eq. (33) predicts the period of oscillations to exceed the GL coherence length ξ , which justifies our usage of the London approximation to derive these results.

The critical spin current density corresponds to $\varphi'(0) = 2k_J$ which together with Eq. (29) gives $j_c^s = 8e(\gamma\psi_0^2/\hbar)k_J$. Using the relations listed above Eq. (33)

one can express it more usefully as

$$j_c^s \simeq j_c^e \left(\frac{\lambda_R}{\Delta_0} \right) \sqrt{3}k_F^2, \quad (34)$$

where $j_c^e = 8e(\psi_0^2/3\hbar)\sqrt{\gamma|\alpha|/3}$ is the GL critical current density [63]. We observe that j_c^s will be small in comparison with j_c^e when either SOC is weak or when μ is near the bottom of the band.

A natural question arises when pondering the results in Fig. 5, namely, to what extent is the oscillatory behavior dependent on the perfect translational invariance of the system. In other words, is this behavior stable with respect to disorder and inhomogeneity? We address this question in Appendix C and find that moderate levels of disorder, modeled as a random spatially varying component of the Josephson coupling J , do not substantially modify our conclusions. Specifically, the spin current injected into a long wire still propagates without dissipation; the main effect of disorder is to add a degree of irregularity to oscillations as illustrated in Fig. 8.

To further support the above predictions of the GL theory we performed analogous calculations within the microscopic model defined by the BdG Hamiltonian Eq. (10) with Rashba SOC implemented via Eq. (2). We employ here the same long strip geometry with d -wave nodes aligned with the principal axes as in Sec. III.B and with periodic boundary conditions along x , open along y , forming topologically a ring. To generate spin current along x we initialize the order parameters according to

$$\Delta_\sigma = \Delta_0 e^{2\pi i \sigma n_v x / L_x}, \quad (35)$$

with n_v denoting the integer vorticity, opposite for two spin projections. For non-zero n_v this choice describes spin-up and down condensates whose relative phase φ winds by $4\pi n_v$ around the ring. When $\lambda_R = 0$ the two condensates are decoupled and one trivially obtains the charge counterflow regime with uniform pure spin current circulating the ring.

The effect of non-zero λ_R on the spin current is illustrated in Fig. 6 where we display fully self-consistent solutions of the BdG theory starting from the ansatz Eq.

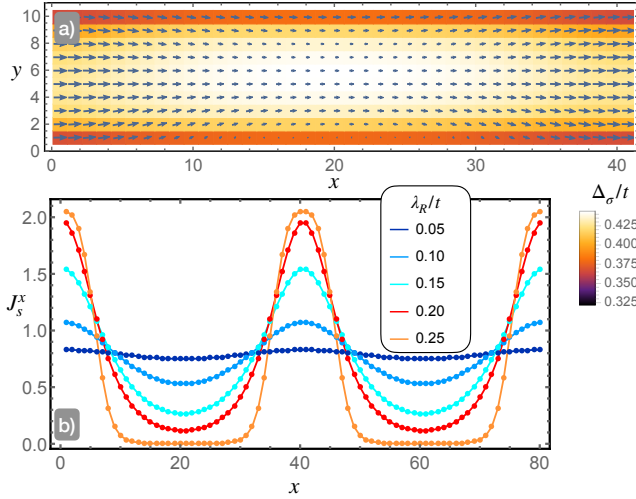


FIG. 6. Effect of Rashba SOC on pure spin supercurrent in a ring geometry modeled as a 80×10 strip with periodic boundary conditions along x , open along y . (a) Order parameter amplitude $|\Delta_\sigma|$ (identical for both spins) shown as the color-scale background and spin current density distribution \mathbf{j}_s indicated by arrows. Both quantities are shown for the left half of the strip, the right half is identical. In order to filter out the edge current we subtracted \mathbf{j}_s calculated for the same parameters with $n_v = 0$. (b) Total spin current J_s^x as a function of the position x along the strip for several representative values of Rashba SOC. The same values of BdG model parameters are used as in Fig. 3 with $n_v = 1$ and $\lambda_R = 0.15$ in panel (a).

(35). We remark that achieving full self-consistency between the BdG Hamiltonian Eq. (10), suitably re-cast in the real space, and the corresponding gap equations (7) is essential for obtaining physical, charge-current conserving solutions. We also note that under this iterative procedure the ansatz Eq. (35) leads to stable solutions with non-zero phase winding, even though the global ground state is in the zero-winding sector.

In agreement with the results of the GL theory we find that SOC brings about spatial oscillations in the spin current J_s^x along the ring, Fig. 6(b). The amplitude of oscillations increases with λ_R , but, importantly, there is no decay in the sense that solutions of the BdG equations are always spatially periodic. This remains true even for very long strips; we were able to simulate systems up to 160×10 in size and various values of n_v , all with similar outcomes.

For larger values of $\lambda_R \gtrsim 0.22$ the spin current is seen to vanish in segments of the strip. We associate this behavior with reaching and exceeding the critical strength of SOC for a given value of the spin current. According to the GL results in a semi-infinite geometry we expect in this regime behaviors like those shown in Fig. 5(b) and (c), respectively. In our present ring geometry the relative phase φ is constrained to wind by $4\pi n_v$ and hence behaviors of this type cannot be reached. Instead, the system shows a transition between the regime with non-

zero J_s^x everywhere along the ring to the regime with $J_s^x = 0$ along parts of the ring. Physically, the phases of two condensates are locked together in these regions and hence $J_s^x = 0$. The relative phase varies rapidly elsewhere, resulting in large J_s^x , in accord with Eq. (29).

C. Persistent spin current in a thin ring

We now consider a ring threaded by magnetic flux Φ , illustrated in Fig. 7. We focus here on the limit where the ring thickness h and width w are both smaller than the magnetic penetration depth. This can be achieved if the ring is made of a thin film such that $h \ll \lambda_L$, the bulk London penetration depth. In this situation the effective in-plane penetration depth will be given by the Pearl length, $\lambda_{\text{Pearl}} = 2\lambda_L^2/h \gg \lambda_L$, making the condition $w \ll \lambda_{\text{Pearl}}$ easy to satisfy.

In the situation described above, the ring material will not quantize the total enclosed flux and the calculations become straightforward as we do not need to consider screening effects. In the non-relativistic limit ($J = 0$) the current densities contributed by the two decoupled condensates follow from Eq. (25) and read

$$\mathbf{j}_\sigma = 4e \frac{\gamma \psi_0^2}{\hbar} (\nabla \varphi_\sigma - \frac{2e}{\hbar c} \mathbf{A}). \quad (36)$$

We represent the flux by $\mathbf{A} = \hat{\theta} \Phi / \ell$, where $\hat{\theta}$ is a unit vector in the azimuthal direction and ℓ denotes the ring circumference. Phases φ_σ are constrained by single-valuedness of the corresponding order parameters ψ_σ . This permits the phase to wind by an integer multiple of 2π around the ring, $\varphi_\sigma(\ell) = \varphi_\sigma(0) + 2\pi n_\sigma$, where n_σ is the integer winding number and we parametrized φ_σ by its position along the ring. Assuming furthermore that phases vary uniformly along the ring we have $\nabla \varphi = 2\pi n_\sigma \hat{\theta} / \ell$. Taken together this allows us to define the ring current

$$I_\sigma = S \hat{\theta} \cdot \mathbf{j}_\sigma = I_0 (n_\sigma - \Phi / \Phi_0), \quad (37)$$

for each spin, where $I_0 = 4eS \frac{\gamma \psi_0^2}{\hbar} \frac{2\pi}{\ell}$ and $S = wh$ is the ring cross section.

To understand the energetics (working still in the $J = 0$ limit) it is useful to write the free energy associated with these currents as

$$F = \frac{1}{2} L_K (I_\uparrow^2 + I_\downarrow^2) + \frac{1}{2} L_G (I_\uparrow + I_\downarrow)^2. \quad (38)$$

The first term represents the energy cost of the superflow and follows directly from the free energy density Eq. (25) with the kinetic inductance defined as $L_K = \hbar^2 \ell / 8e^2 S \gamma \psi_0^2$. The second term expresses the energy stored in the magnetic field B generated by the total electric current $I = I_\uparrow + I_\downarrow$ flowing in the ring with L_G denoting its geometric inductance and follows from the last term in Eq. (23). The precise value of L_G depends

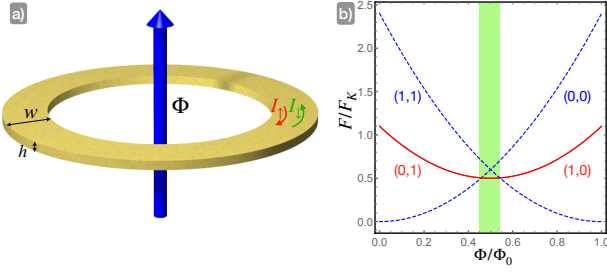


FIG. 7. (a) A SC ring threaded by magnetic flux Φ . Red and green arrows illustrate the charge counterflow regime that becomes energetically favorable when Φ is close to a half-integer multiple of the SC flux quantum at weak SOC. (b) Free energy Eq. (38) as a function of the inserted flux Φ/Φ_0 . Various branches correspond to winding numbers $(n_\uparrow, n_\downarrow)$ as indicated and $F_K = \frac{1}{2}L_K I_0^2$. The green-shaded region marks the range of flux values where charge counterflow solutions minimize the free energy and are thus stable.

on the details of the ring geometry. For the illustration purposes we can estimate it by the well-known Kirchhoff formula $L_G \simeq (8\pi\ell/c^2)[\ln(\ell/\rho) - 1.508]$ for the self-inductance of a ring with circular cross section of radius ρ and circumference ℓ , accurate in the limit $\ell \gg \rho$ [64].

A simple but important observation follows from Eq. (38): In situations when the magnitudes of I_\uparrow and I_\downarrow are equal, the free energy is minimized when $I_\uparrow = -I_\downarrow$ because then the second term vanishes. This situation corresponds to the *charge counterflow* regime in which there is a pure spin current flowing in the wire. The physical reason behind this interesting conclusion is simply that while charge current incurs an energy cost due to the induced magnetic field, spin current does not.

A practical route towards the realization of the charge counterflow regime offers itself based on the above insight. Fig. 7(b) shows the behavior of the free energy Eq. (38) as a function of the flux Φ with various branches representing different vorticities $(n_\uparrow, n_\downarrow)$. In equilibrium the system will be on the branch that minimizes F for the given flux. We observe that close to $\Phi = \Phi_0/2$ the global minimum occurs when $(n_\uparrow, n_\downarrow) = (1, 0)$ or $(0, 1)$. In view of Eq. (37) these solutions correspond to spin-up and down currents flowing in the opposite directions. At exact half flux quantum this implies pure spin persistent currents flowing in clockwise and counterclockwise direction for $(n_\uparrow, n_\downarrow) = (1, 0)$ and $(0, 1)$, respectively. Solutions with winding numbers $(1, 1)$ and $(0, 0)$ correspond to conventional (unpolarized) persistent currents but are higher in energy by $\frac{1}{2}L_G I_0^2$.

We thus conclude that in the non-relativistic limit one can realize pure spin supercurrent in a ring threaded by half-integer number of magnetic flux quanta. The two states with this property minimize the global free energy and are thus truly persistent in the sense that spin currents cannot decay even as a matter of principle.

A natural question arises: How does a departure from the non-relativistic limit affect this result? Persistent

spin currents discussed above involve solutions with different winding numbers n_σ for the two spin projections. Therefore, the phase difference $\varphi_\uparrow - \varphi_\downarrow$ in the argument of the J term in the free energy Eq. (25) will also wind around the ring. This implies an energy cost $\Delta F_J \simeq JS\ell$ compared to the state with $\varphi_\uparrow = \varphi_\downarrow$. On this basis we expect the persistent spin current solutions to be energetically favored as long as $\Delta F_J \lesssim \frac{1}{2}L_G I_0^2$. This places an upper bound on the strength of SOC that can be tolerated, expressed as $J < J_c \simeq L_G I_0^2 / 2S\ell$. Using Eq. (26) and various relations listed above Eq. (33) one can translate this into a condition $\lambda_R < \lambda_{Rc}$ with

$$\lambda_{Rc}^2 \simeq \frac{4\pi^2 \Delta_0^2}{k_F^4} \left(\frac{\xi}{\lambda_L} \right)^2 \frac{S}{\ell^2} \left[\ln \frac{\ell}{\rho} - 1.508 \right]. \quad (39)$$

Here $\lambda_L^2 = \hbar^2 c^2 / 8\pi(2e)^2 \gamma \psi_0^2$ is the London penetration depth and $\rho \simeq \sqrt{S/\pi}$ is the effective radius of the ring cross section area.

We thus find that persistent spin current solutions can be favored even away from the non-relativistic limit as long as the SOC strength satisfies $\lambda_R < \lambda_{Rc}$ with λ_{Rc} given in Eq. (39). To get a sense for the relevant magnitudes we consider a ring with radius $R = 1\mu\text{m}$ and a rectangular cross section with $(w, h) = (0.1, 0.01)\mu\text{m}$. If we furthermore assume representative parameter values $\xi/\lambda_L \approx 1$ and $k_F = 0.5$ then Eq. (39) gives $\lambda_{Rc} \simeq 0.3\Delta_0$. Hence we conclude that under rather generic conditions there will exist a reasonable window of permissible SOC strength in which pure persistent spin current can be induced in a ring by half-integer flux. This window, according to Eq. (39), becomes wider for smaller samples, a useful property that can be used to detect and tune the effect experimentally.

We note, finally, that the pure spin supercurrent predicted to occur near the half-flux quantum can be detected by a simple magnetization measurement, i.e. no direct spin-current detection is required. Consider increasing Φ from zero. Initially, the system will be on the $(0,0)$ branch in Fig. 7(b) and will hence support charge current proportional to Φ according to Eq. (37), accompanied with the corresponding magnetization, also proportional to Φ . Sufficiently close to $\Phi_0/2$ the system will switch to the $(1,0)$ or $(0,1)$ branch. Here the charge current is near zero and so is the magnetization. The signature of a pure spin supercurrent is therefore given by a range of near-vanishing magnetization around $\Phi = \Phi_0/2$ – this is in contrast to the normal case where magnetization is maximal in this region.

V. OUTLOOK

Efficient generation, manipulation, and detection of spin currents is one of the key goals of the field of spintronics. Our work establishes superconducting altermagnets as a new viable platform for achieving some of these goals in a setting where spin dissipation, a key challenge

that must be faced in normal metal and semiconductor devices, is not an issue. We have demonstrated that SC altermagnets are capable of carrying spin-polarized currents without dissipation over arbitrarily long distances, even in the presence of SOC and magnetic disorder which generally lead to short spin life times in non-superconducting materials.

The above advances are rooted in two key insights: (i) the characteristic spin-split band structure of metallic altermagnets makes them uniquely susceptible to an exotic form of spin-triplet p -wave superconductivity, perfectly suited for generation and transport of spin currents; and (ii) the resulting spin currents are persistent in that they flow in the equilibrium state of the system, and hence, once established they cannot decay. This last property is well documented in the context of conventional charge supercurrents. Here we showed that with small modifications it extends to spin supercurrents. We found that while perturbations away from the strictly non-relativistic limit (e.g. SOC and magnetic disorder) can cause spin current to undergo spatial oscillations and fluctuations, crucially, it still propagates over arbitrary distances without any overall decay. The difference is rooted in the fact that unlike charge, spin is not a conserved quantity in real materials and hence spin polarization is allowed to fluctuate. Nevertheless, the structure of the theory still does not permit dissipation to occur simply because the system with spin supercurrent is already in the state of the lowest free energy compatible with its boundary conditions.

A key challenge going forward lies in discovery of a suitable family of altermagnets with an intrinsic superconducting instability occurring at temperatures that are not too low to prevent practical applications. Although no SC altermagnets have yet been identified, it is to be noted that many existing and predicted altermagnets are good metals. With zero net magnetization enforced by spin group symmetry such metals are generically susceptible to Cooper pair formation in the presence of a weak attractive interaction. Importantly, our work shows that the highly coveted spin-triplet SC order is expected to occur due to the underlying spin-split band structure and does not require any exotic pairing mechanism; the conventional retarded phonon-induced attraction is perfectly adequate for the task. In addition, it is known that the presence of magnetism in a material is not necessarily inimical to superconductivity: high- T_c cuprates and some iron-based superconductors famously emerge from doped antiferromagnets [65]. Likewise, several ferromagnetic superconductors have been reported in the literature, including a number of f -electron compounds such as CeCu₂Si₂ [66], as well as UGe₂, URhGe, and UCoGe [67].

It should be noted that Cooper pairing at nonzero center-of-mass momentum [68] has been discussed as a possible alternative to the zero-momentum spin-triplet p -wave SC order in altermagnets. A discovery of such a pair density or Fulde-Ferrell-Larkin-Ovchinnikov (FFLO) state

would be perhaps as exciting as the spin-triplet p -wave order, although its utility in spintronics or other practical applications is yet to be understood. In either case search for superconducting altermagnets holds promise of exciting future discoveries.

The possibility of induced SC order, of the type useful for spintronic applications, in a known altermagnet by the proximity effect with an established superconductor is an interesting open question. On symmetry grounds one could imagine that proximity-inducing spin-triplet p -wave order using a conventional spin-singlet superconductor might be challenging. However, a clever scheme that would leverage interfacial SOC or surface-state engineering could perhaps bring about such a feat, thus providing a shortcut towards useful artificially engineered SC altermagnets.

ACKNOWLEDGMENTS

We are grateful to Tomas Jungwirth, Vic Law, Alan MacDonald, Joel Moore, Andreas Schnyder and Libor Smejkal for illuminating discussions and correspondence. This research was supported in part by NSERC, CIFAR, and the Canada First Research Excellence Fund, Quantum Materials and Future Technologies Program.

Appendix A: Superfluid density tensor

Various equivalent expressions can be found in the literature for the superfluid density of a BCS superconductor. Here we use the expression derived in two different ways in Refs. [69, 70], valid for a 2D lattice superconductor with a normal state dispersion $\xi_{\mathbf{k}}$ and gap function $\Delta_{\mathbf{k}}$. Adapted to our model of a d -wave altermagnet it reads

$$[\hat{\rho}_{\sigma}]_{\alpha\beta} = \frac{e}{2\hbar^2 S} \sum_{\mathbf{k}} \left[\frac{\partial^2 \xi_{\mathbf{k}\sigma}}{\partial k_{\alpha} \partial k_{\beta}} \left(1 - \frac{\xi_{\mathbf{k}\sigma}}{E_{\mathbf{k}\sigma}} \tanh \frac{1}{2} \beta E_{\mathbf{k}\sigma} \right) - \frac{1}{2} \beta \frac{\partial \xi_{\mathbf{k}\sigma}}{\partial k_{\alpha}} \frac{\partial \xi_{\mathbf{k}\sigma}}{\partial k_{\beta}} \text{sech}^2 \frac{1}{2} \beta E_{\mathbf{k}\sigma} \right]. \quad (\text{A1})$$

Here the sum is over the Brillouin zone, $E_{\mathbf{k}\sigma} = \sqrt{\xi_{\mathbf{k}\sigma}^2 + \Delta_{\sigma}^2 |S_{\mathbf{k}\sigma}|^2}$ is the quasiparticle excitation energy and S denotes the area of the system.

For a fully gapped superconductor the expression simplifies in the $T \rightarrow 0$ limit and gives

$$[\hat{\rho}_{\sigma}]_{\alpha\beta} = \frac{e}{2\hbar^2 S} \sum_{\mathbf{k}} \frac{\partial^2 \xi_{\mathbf{k}\sigma}}{\partial k_{\alpha} \partial k_{\beta}} \left(1 - \frac{\xi_{\mathbf{k}\sigma}}{E_{\mathbf{k}\sigma}} \right). \quad (\text{A2})$$

If we further assume that the gap is small compared to the Fermi energy and consider electron filling near the bottom of the band, Eq. (A2) can be approximated as

$$[\hat{\rho}_{\sigma}]_{\alpha\beta} \simeq [M_{\sigma}^{-1}]_{\alpha\beta} \frac{e}{2S} \sum_{\mathbf{k}} \left(1 - \frac{\xi_{\mathbf{k}\sigma}}{|\xi_{\mathbf{k}\sigma}|} \right). \quad (\text{A3})$$

Here $[M_\sigma^{-1}]_{\alpha\beta} = \hbar^{-2} \partial^2 \xi_{\mathbf{k}\sigma} / \partial k_\alpha \partial k_\beta$ is the inverse effective mass tensor and the sum represents the electron density n_e per spin.

For the altermagnetic energy dispersion that follows from Eq. (1) we have

$$M_\sigma^{-1} \simeq \frac{2}{\hbar^2} \begin{pmatrix} t + \sigma\eta & 0 \\ 0 & t - \sigma\eta \end{pmatrix}, \quad (\text{A4})$$

which then leads directly to Eq. (17).

Appendix B: Physics of the $\psi_\uparrow^* \psi_\downarrow$ term

The $\psi_\uparrow^* \psi_\downarrow$ term in GL free energy Eq. (23) is symmetry allowed for the two helical phases listed in Table 1 but is disallowed for the chiral phases. To see this we consider its behavior under C_{z4} rotation. It is useful to note that the z -component of the total angular momentum of the equal-spin triplet order parameters is $J_z = (0, 0, 2, -2)$ for $(p_-^\uparrow, p_+^\downarrow, p_+^\uparrow, p_-^\downarrow)$, respectively. Under C_{z4} such order parameters transform as $\psi \rightarrow e^{iJ_z\pi/2}\psi$.

It follows that the bilinear term $D(\psi_\uparrow^* \psi_\downarrow + \text{c.c.})$ in Eq. (23) is invariant under C_{z4} if the two order parameters represent $p_-^\uparrow \otimes p_+^\downarrow$ or $p_+^\uparrow \otimes p_-^\downarrow$ configurations, that is, the two helical phases. On the other hand, the bilinear term is odd under C_{z4} for the two chiral combinations $p_-^\uparrow \otimes p_-^\downarrow$ and $p_+^\uparrow \otimes p_+^\downarrow$. In this case the lowest-order coupling involves a quartic term $D_4(\psi_\uparrow^{2*} \psi_\downarrow^2 + \text{c.c.})$.

In the presence of weak SOC we expect $D \propto \lambda^2$ and $D_4 \propto \lambda^4$ because the two terms represent tunneling of one and two Cooper pairs between two spin sectors, respectively. In the following we use the microscopic BdG model defined in Sec. II to explicitly evaluate the Josephson coupling $J = D\psi_0^2$ for the helical $p_-^\uparrow \otimes p_+^\downarrow$ phase of a d -wave altermagnet. Specifically, we consider the normal-state lattice Hamiltonian defined by Eqs. (1) and (2) in the presence of attractive interaction (6), decoupled in the triplet channel as shown in Eq. (9b).

We obtain J by expanding the free energy of the BdG model

$$F(\varphi) = E_0 - \frac{2}{\beta} \sum_{\mathbf{k}, a} \ln \left[2 \cosh \left(\frac{1}{2} \beta E_{\mathbf{k}a}(\varphi) \right) \right], \quad (\text{B1})$$

to leading order in the relative phase φ between the two order parameters. Here β denotes the inverse temperature, E_0 contains terms independent of φ and $E_{\mathbf{k}a}(\varphi)$ are two positive eigenvalues of the 4×4 BdG matrix Hamiltonian Eq. (11). For the helical $p_-^\uparrow \otimes p_+^\downarrow$ phase these can be expressed as

$$E_{\mathbf{k}a}^2(\varphi) = \xi_{\mathbf{k}}^2 + \eta_{\mathbf{k}}^2 + |\lambda_{\mathbf{k}}|^2 + |\Delta_{\mathbf{k}}|^2 + 2aD_{\mathbf{k}}(\varphi), \quad (\text{B2})$$

with $a = \pm$,

$$D_{\mathbf{k}}^2(\varphi) = \xi_{\mathbf{k}}^2(\eta_{\mathbf{k}}^2 + |\lambda_{\mathbf{k}}|^2) + \Im(\lambda_{\mathbf{k}} \Delta_{\mathbf{k}})^2 \quad (\text{B3})$$

and

$$\begin{aligned} \xi_{\mathbf{k}} &= -2t(\cos k_x + \cos k_y) - \mu, \\ \eta_{\mathbf{k}} &= -2\eta(\cos k_x - \cos k_y), \\ \lambda_{\mathbf{k}} &= \lambda_R e^{i\varphi/2} (\sin k_y + i \sin k_x) \\ \Delta_{\mathbf{k}} &= \Delta_0 (\sin k_x + i \sin k_y). \end{aligned} \quad (\text{B4})$$

In order to make headway we now focus on the chemical potential near the bottom of the band and expand $\xi_{\mathbf{k}}$ and $\eta_{\mathbf{k}}$ in Eq. (B4) to leading order in small momentum k ,

$$\xi_{\mathbf{k}} \simeq t(k^2 - k_F^2), \quad \eta_{\mathbf{k}} \simeq \eta(k_x^2 - k_y^2), \quad (\text{B5})$$

where $k_F = \sqrt{(\mu + 4t)/t}$ is the Fermi momentum. The remaining quantities in Eq. (B4) are similarly expanded near the Fermi level, e.g.

$$\Delta_{\mathbf{k}} \simeq \Delta_0(k_x + ik_y) \approx \Delta_0 k_F e^{i\alpha_{\mathbf{k}}}, \quad (\text{B6})$$

where $\alpha_{\mathbf{k}}$ is the angle between vector \mathbf{k} and the k_x axis.

We note that the entire φ dependence of the free energy is contained in the last term of Eq. (B3) which is simplified in this approximation as

$$\Im(\lambda_{\mathbf{k}} \Delta_{\mathbf{k}})^2 \simeq \lambda_R^2 \Delta_0^2 k_F^4 \cos^2(\varphi/2), \quad (\text{B7})$$

We expect the leading behavior of the free energy to be of the form $F(\varphi) \propto \lambda_R^2 \cos \varphi$. To isolate this term we now focus on the free energy derivative $F'(\varphi)$ which can be expressed as

$$F' = - \sum_{\mathbf{k}, a} \frac{1}{2E_{\mathbf{k}a}} \frac{\partial E_{\mathbf{k}a}^2}{\partial \varphi} \tanh \frac{1}{2} \beta E_{\mathbf{k}a}. \quad (\text{B8})$$

The phase derivative can be written as

$$\frac{\partial E_{\mathbf{k}a}^2}{\partial \varphi} = -\frac{1}{2} a \lambda_R^2 \Delta_0^2 k_F^4 \frac{\sin \varphi}{D_{\mathbf{k}}(\varphi)}. \quad (\text{B9})$$

Given that this term is proportional to λ_R^2 and we are interested in the result to this order we can evaluate the sum in Eq. (B8) by taking $\lambda_R \rightarrow 0$ in the rest of the expression. This simplifies things considerably and we obtain, in the limit of zero temperature T ,

$$F' \simeq -\frac{1}{2} \lambda_R^2 \Delta_0^2 k_F^4 \sum_{\mathbf{k}, a} \frac{a \sin \varphi}{|\xi_{\mathbf{k}} \eta_{\mathbf{k}}| \sqrt{(\xi_{\mathbf{k}} + a\eta_{\mathbf{k}})^2 + \Delta_0^2}}. \quad (\text{B10})$$

Hence we see that to leading order $F' \propto \lambda_R^2 \sin \varphi$, as expected.

To find the proportionality constant we must evaluate the remaining sum over \mathbf{k} . The leading contribution can be estimated already in the limit of zero spin splitting η . Taking the limit $\eta \rightarrow 0$ we find

$$F' \simeq \lambda_R^2 \Delta_0^2 k_F^4 \sin \varphi \sum_{\mathbf{k}} \frac{1}{(\xi_{\mathbf{k}}^2 + \Delta_0^2)^{3/2}}. \quad (\text{B11})$$

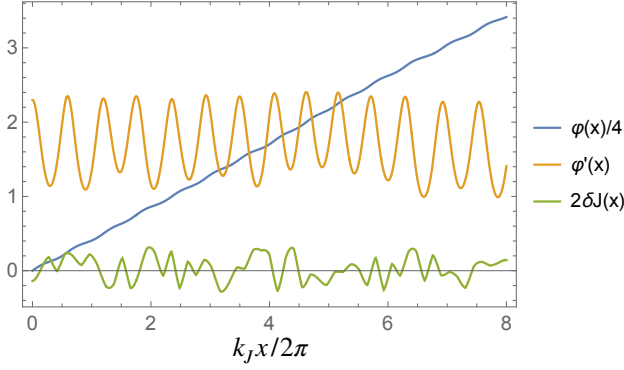


FIG. 8. Spin current in a long wire calculated from the GL theory with a spatially varying random internal Josephson coupling described in the text. We used $M = 42$ random values with $\langle \delta J^2 \rangle^{1/2} = 0.3J_0$ and $\varphi'(0) = 2.3$.

We evaluate the sum and arrive at

$$F' \simeq \frac{\lambda_R^2 k_F^4}{4\pi t} \sin \varphi. \quad (\text{B12})$$

The expression is valid for $\lambda_R \lesssim \Delta_0$ and for the chemical potential near the bottom of the band such that the expansion of $\xi_{\mathbf{k}}$ in Eq. (B5) is accurate. The last condition is met when $k_F \lesssim 1$.

We thus conclude that to the leading order in the phase difference the free energy can be written as

$$F(\varphi) \simeq F_0 - J \cos \varphi, \quad J \simeq \frac{\lambda_R^2 k_F^4}{4\pi t}, \quad (\text{B13})$$

where F_0 is independent of φ . We note that because of the 4π factor in the denominator even a fairly significant SOC strength $\lambda_R \sim t$ will tend to yield relatively small values of J . In addition, J can be further suppressed by going to low electron density limit where $k_F \ll 1$. We conclude that generically one may expect the linear coupling between spin-up and spin-down order parameters to be parametrically small compared to other energy scales in the problem.

We note that a similar calculation can be performed for the $p_+^\uparrow \otimes p_-^\downarrow$ helical phase. In this case $\Im(\lambda_{\mathbf{k}} \Delta_{\mathbf{k}})$ in Eq. (B3) is replaced by $\Im(\lambda_{\mathbf{k}} \Delta_{\mathbf{k}}^*)$. One obtains the same expression (B13) for the free energy except with a modified $J \simeq -\lambda_R^2 k_F^6 / 192t$. Finally, the calculation can be performed for the two chiral phases listed in Table 1. In this case the form of the BdG energy eigenvalues is different from Eq. (C2) and the calculation to the same order gives $J = 0$, consistent with the expectation that the leading contribution is fourth order in λ_R .

Appendix C: Spin current with random J

To model disorder we consider free energy density Eq. (26) with the internal Josephson coupling containing a spatially varying component

$$J(x) = J_0 + \delta J(x). \quad (\text{C1})$$

Here $\delta J(x)$ is generated by smoothly interpolating M random numbers $w(x_j)$ drawn from a uniform distribution $[-r, r]$ at spatial positions $x_j = jL/M$ with $j = 1, \dots, M$. The corresponding Euler-Lagrange equation

$$\frac{d^2 \varphi}{dx^2} + k_J^2 [1 + \zeta(x)] \sin \varphi = 0, \quad (\text{C2})$$

with $\zeta(x) = \delta J(x)/J_0$ is then solved numerically subject to boundary conditions at $x = 0$ just like in Sec. IV.B. A representative solution is displayed in Fig. 8. We find that non-decaying oscillatory solutions of the type displayed generally persist for small-amplitude disorder. When the injected current density is close to the critical value j_c^s we sometimes find that a large fluctuation in δJ can switch the behavior between two types displayed in Figs. 5(a) and (c). Nevertheless, the current remains undamped in all cases.

-
- [1] R. F. Broom, “An upper limit for the resistivity of a superconducting film,” *Nature* **190**, 992–993 (1961).
 - [2] J. File and R. G. Mills, “Observation of persistent current in a superconducting solenoid,” *Phys. Rev. Lett.* **10**, 93–96 (1963).
 - [3] Igor Žutić, Jaroslav Fabian, and S. Das Sarma, “Spintronics: Fundamentals and applications,” *Rev. Mod. Phys.* **76**, 323–410 (2004).
 - [4] Jairo Sinova, Sergio O. Valenzuela, J. Wunderlich, C. H. Back, and T. Jungwirth, “Spin hall effects,” *Rev. Mod. Phys.* **87**, 1213–1260 (2015).
 - [5] Jacob Linder and Jason W. A. Robinson, “Superconducting spintronics,” *Nature Physics* **11**, 307–315 (2015).
 - [6] Matthias Eschrig, “Spin-polarized supercurrents for spintronics: a review of current progress,” *Reports on Progress in Physics* **78**, 104501 (2015).
 - [7] Kun-Rok Jeon, Chiara Ciccarelli, Andrew J. Ferguson, Hidekazu Kurebayashi, Lesley F. Cohen, Xavier Montiel, Matthias Eschrig, Jason W. A. Robinson, and Mark G. Blamire, “Enhanced spin pumping into superconductors provides evidence for superconducting pure spin currents,” *Nature Materials* **17**, 499–503 (2018).
 - [8] Nathan Satchell and Norman O. Birge, “Supercurrent in ferromagnetic Josephson junctions with heavy metal interlayers,” *Phys. Rev. B* **97**, 214509 (2018).

- [9] Kun-Rok Jeon, Chiara Ciccarelli, Hidekazu Kurebayashi, Lesley F. Cohen, Xavier Montiel, Matthias Eschrig, Sachio Komori, Jason W. A. Robinson, and Mark G. Blamire, “Exchange-field enhancement of superconducting spin pumping,” *Phys. Rev. B* **99**, 024507 (2019).
- [10] Isidoro Martínez, Petra Högl, César González-Ruano, Juan Pedro Cascales, Coriolan Tiusan, Yuan Lu, Michel Hehn, Alex Matos-Abiague, Jaroslav Fabian, Igor Žutić, and Farkhad G. Aliev, “Interfacial spin-orbit coupling: A platform for superconducting spintronics,” *Phys. Rev. Appl.* **13**, 014030 (2020).
- [11] Kun-Rok Jeon, Xavier Montiel, Sachio Komori, Chiara Ciccarelli, James Haigh, Hidekazu Kurebayashi, Lesley F. Cohen, Alex K. Chan, Kilian D. Stenning, Chang-Min Lee, Matthias Eschrig, Mark G. Blamire, and Jason W. A. Robinson, “Tunable pure spin supercurrents and the demonstration of their gateability in a spin-wave device,” *Phys. Rev. X* **10**, 031020 (2020).
- [12] James Jun He, Kanta Hiroki, Keita Hamamoto, and Naoto Nagaosa, “Spin supercurrent in two-dimensional superconductors with rashba spin-orbit interaction,” *Communications Physics* **2**, 128 (2019).
- [13] M. A. Silaev, I. V. Bobkova, and A. M. Bobkov, “Odd triplet superconductivity induced by a moving condensate,” *Phys. Rev. B* **102**, 100507 (2020).
- [14] X. Montiel and M. Eschrig, “Spin current injection via equal-spin cooper pairs in ferromagnet/superconductor heterostructures,” *Phys. Rev. B* **107**, 094513 (2023).
- [15] Simran Chourasia, Lina Johnsen Kamra, Irina V. Bobkova, and Akashdeep Kamra, “Generation of spin-triplet cooper pairs via a canted antiferromagnet,” *Phys. Rev. B* **108**, 064515 (2023).
- [16] G. A. Bobkov, A. M. Bobkov, and I. V. Bobkova, “Spin supercurrent in superconductor/ferromagnet van der waals heterostructures,” *Phys. Rev. B* **110**, 104506 (2024).
- [17] Kyo-Hoon Ahn, Atsushi Hariki, Kwan-Woo Lee, and Jan Kuneš, “Antiferromagnetism in ruo 2 as d-wave pomeranchuk instability,” *Physical Review B* **99**, 184432 (2019).
- [18] Satoru Hayami, Yuki Yanagi, and Hiroaki Kusunose, “Momentum-dependent spin splitting by collinear antiferromagnetic ordering,” *Journal of the Physical Society of Japan* **88**, 123702 (2019).
- [19] Libor Šmejkal, Jairo Sinova, and Tomas Jungwirth, “Beyond conventional ferromagnetism and antiferromagnetism: A phase with nonrelativistic spin and crystal rotation symmetry,” *Phys. Rev. X* **12**, 031042 (2022).
- [20] Libor Šmejkal, Jairo Sinova, and Tomas Jungwirth, “Emerging research landscape of altermagnetism,” *Phys. Rev. X* **12**, 040501 (2022).
- [21] Igor Mazin (The PRX Editors), “Editorial: Altermagnetism—a new punch line of fundamental magnetism,” *Phys. Rev. X* **12**, 040002 (2022).
- [22] Bei Jiang, Mingzhe Hu, Jianli Bai, Ziyin Song, Chao Mu, Gexing Qu, Wan Li, Wenliang Zhu, Hanqi Pi, Zhongxu Wei, *et al.*, “A metallic room-temperature d-wave altermagnet,” *Nature Physics* , 1–6 (2025).
- [23] A. Kitz, “Über die symmetriegruppen von spinverteilungen von,” *physica status solidi (b)* **10**, 455–466 (1965).
- [24] WF Brinkman and Roger James Elliott, “Theory of spin-space groups,” *Proceedings of the Royal Society of London. Series A. Mathematical and Physical Sciences* **294**, 343–358 (1966).
- [25] W. Brinkman and R. J. Elliott, “Space Group Theory for Spin Waves,” *Journal of Applied Physics* **37**, 1457–1459 (1966).
- [26] D.B. Litvin and W. Opechowski, “Spin groups,” *Physica* **76**, 538–554 (1974).
- [27] A. Corticelli, R. Moessner, and P. A. McClarty, “Spin-space groups and magnon band topology,” *Phys. Rev. B* **105**, 064430 (2022).
- [28] Hana Schiff, Alberto Corticelli, Afonso Guerreiro, Judit Romhányi, and Paul A McClarty, “The crystallographic spin point groups and their representations,” *SciPost Physics* **18**, 109 (2025).
- [29] Kirill Parshukov and Andreas P. Schnyder, “Exotic superconducting states in altermagnets,” (2025), [arXiv:2507.10700 \[cond-mat.supr-con\]](https://arxiv.org/abs/2507.10700).
- [30] Di Zhu, Zheng-Yang Zhuang, Zhigang Wu, and Zhongbo Yan, “Topological superconductivity in two-dimensional altermagnetic metals,” *Phys. Rev. B* **108**, 184505 (2023).
- [31] Bjørnulf Brekke, Arne Brataas, and Asle Sudbø, “Two-dimensional altermagnets: Superconductivity in a minimal microscopic model,” *Phys. Rev. B* **108**, 224421 (2023).
- [32] Tsz Fung Heung and Marcel Franz, “Probing topological degeneracy on a torus using superconducting altermagnets,” (2024), [arXiv:2411.17964 \[cond-mat.supr-con\]](https://arxiv.org/abs/2411.17964).
- [33] Vanuildo S. de Carvalho and Hermann Freire, “Unconventional superconductivity in altermagnets with spin-orbit coupling,” *Phys. Rev. B* **110**, L220503 (2024).
- [34] Kristoffer Leraand, Kristian Maeland, and Asle Sudbø, “Phonon-mediated spin-polarized superconductivity in altermagnets,” (2025), [arXiv:2502.08704 \[cond-mat.supr-con\]](https://arxiv.org/abs/2502.08704).
- [35] Fayuan Zhang, Xingkai Cheng, Zhouyi Yin, Changchao Liu, Liwei Deng, Yuxi Qiao, Zheng Shi, Shuxuan Zhang, Junhao Lin, Zhengtai Liu, Mao Ye, Yaobo Huang, Xiangyu Meng, Cheng Zhang, Taichi Okuda, Kenya Shimada, Shengtao Cui, Yue Zhao, Guang-Han Cao, Shan Qiao, Junwei Liu, and Chaoyu Chen, “Crystal-symmetry-paired spin-valley locking in a layered room-temperature antiferromagnet,” (2024), [arXiv:2407.19555 \[cond-mat.str-el\]](https://arxiv.org/abs/2407.19555).
- [36] J. Krempaský, L. Šmejkal, S. W. D’Souza, M. Hajlaoui, G. Springholz, K. Uhlířová, F. Alarab, P. C. Constantinou, V. Strocov, D. Usanov, W. R. Pudelpko, R. González-Hernández, A. Birk Hellenes, Z. Jansa, H. Reichlová, Z. Šobán, R. D. Gonzalez Betancourt, P. Wadley, J. Sinova, D. Kriegner, J. Minár, J. H. Dil, and T. Jungwirth, “Altermagnetic lifting of kramers spin degeneracy,” *Nature* **626**, 517–522 (2024).
- [37] Suyoung Lee, Sangjae Lee, Saegyeol Jung, Jiwon Jung, Donghan Kim, Yeonjae Lee, Byeongjun Seok, Jaeyoung Kim, Byeong Gyu Park, Libor Šmejkal, Chang-Jong Kang, and Changyoung Kim, “Broken kramers degeneracy in altermagnetic mnte,” *Phys. Rev. Lett.* **132**, 036702 (2024).
- [38] Olena Fedchenko, Jan Minár, Akashdeep Akashdeep, Sunil Wilfred D’Souza, Dmitry Vasilyev, Olena Tkach, Lukas Odenbreit, Quynh Nguyen, Dmytro Kutnyakhov, Nils Wind, Lukas Wenthau, Markus Scholz, Kai Rossnagel, Moritz Hoesch, Martin Aeschlimann, Benjamin Stadtmüller, Mathias Kläui, Gerd Schönhense, Tomas Jungwirth, Anna Birk Hellenes, Gerhard Jakob, Libor Šmejkal, Jairo Sinova, and Hans-Joachim Elmers, “Ob-

- servation of time-reversal symmetry breaking in the band structure of altermagnetic RuO_2 ,” *Science Advances* **10**, ead4883 (2024).
- [39] Sonka Reimers, Lukas Odenbreit, Libor Šmejkal, Vladimir N. Strocov, Procopios Constantinou, Anna B. Hellenes, Rodrigo Jaeschke Ubiergo, Warley H. Campos, Venkata K. Bharadwaj, Atasi Chakraborty, Thibaud Denneulin, Wen Shi, Rafal E. Dunin-Borkowski, Suvadip Das, Mathias Kläui, Jairo Sinova, and Martin Jourdan, “Direct observation of altermagnetic band splitting in CrSb thin films,” *Nature Communications* **15**, 2116 (2024).
- [40] Jianyang Ding, Zhicheng Jiang, Xiuhua Chen, Zicheng Tao, Zhengtai Liu, Tongrui Li, Jishan Liu, Jianping Sun, Jinguang Cheng, Jiayu Liu, Yichen Yang, Runfeng Zhang, Liwei Deng, Wenchuan Jing, Yu Huang, Yuming Shi, Mao Ye, Shan Qiao, Yilin Wang, Yanfeng Guo, Donglai Feng, and Dawei Shen, “Large band splitting in g -wave altermagnet CrSb ,” *Phys. Rev. Lett.* **133**, 206401 (2024).
- [41] Guowei Yang, Zhanghuan Li, Sai Yang, Jiyuan Li, Hao Zheng, Weifan Zhu, Ze Pan, Yifu Xu, Saizheng Cao, Wenxuan Zhao, Anupam Jana, Jiawen Zhang, Mao Ye, Yu Song, Lun-Hui Hu, Lexian Yang, Jun Fujii, Ivana Vobornik, Ming Shi, Huiqiu Yuan, Yongjun Zhang, Yuanfeng Xu, and Yang Liu, “Three-dimensional mapping of the altermagnetic spin splitting in CrSb ,” (2025), [arXiv:2405.12575 \[cond-mat.mtrl-sci\]](https://arxiv.org/abs/2405.12575).
- [42] Makoto Naka, Satoru Hayami, Hiroaki Kusunose, Yuki Yanagi, Yukitoshi Motome, and Hitoshi Seo, “Spin current generation in organic antiferromagnets,” *Nature Communications* **10**, 4305 (2019).
- [43] Lin-Ding Yuan, Zhi Wang, Jun-Wei Luo, Emmanuel I. Rashba, and Alex Zunger, “Giant momentum-dependent spin splitting in centrosymmetric low- z antiferromagnets,” *Phys. Rev. B* **102**, 014422 (2020).
- [44] Igor I. Mazin, Klaus Koepernik, Michelle D. Johannes, Rafael González-Hernández, and Libor Šmejkal, “Prediction of unconventional magnetism in doped $\text{FeSb}_{1-x}\text{Te}_x$,” *Proceedings of the National Academy of Sciences* **118**, e2108924118 (2021).
- [45] Sayantika Bhowal and Nicola A. Spaldin, “Magnetic octupoles as the order parameter for unconventional antiferromagnetism,” (2022), [arXiv:2212.03756 \[cond-mat.str-el\]](https://arxiv.org/abs/2212.03756).
- [46] Yaqian Guo, Hui Liu, Oleg Janson, Ion Cosma Fulga, Jeroen van den Brink, and Jorge I. Facio, “Spin-split collinear antiferromagnets: A large-scale ab-initio study,” *Materials Today Physics* **32**, 100991 (2023).
- [47] I. V. Maznichenko, A. Ernst, D. Maryenko, V. K. Dugaev, E. Ya. Sherman, P. Buczek, S. S. P. Parkin, and S. Ostanin, “Fragile altermagnetism and orbital disorder in mott insulator LaTiO_3 ,” *Phys. Rev. Mater.* **8**, 064403 (2024).
- [48] Yichen Liu, Junxi Yu, and Cheng-Cheng Liu, “Twisted magnetic van der Waals bilayers: An ideal platform for altermagnetism,” *Phys. Rev. Lett.* **133**, 206702 (2024).
- [49] Jabir Ali Ouassou, Arne Brataas, and Jacob Linder, “dc josephson effect in altermagnets,” *Phys. Rev. Lett.* **131**, 076003 (2023).
- [50] Michał Papaj, “Andreev reflection at the altermagnet-superconductor interface,” *Phys. Rev. B* **108**, L060508 (2023).
- [51] C. W. J. Beenakker and T. Vakhel, “Phase-shifted andreev levels in an altermagnet josephson junction,” *Phys. Rev. B* **108**, 075425 (2023).
- [52] Hans Glöckner Gil, Bjørnulf Brekke, Jacob Linder, and Arne Brataas, “Quasiclassical theory of superconducting spin-splitter effects and spin-filtering via altermagnets,” *Phys. Rev. B* **110**, L140506 (2024).
- [53] Song-Bo Zhang, Lun-Hui Hu, and Titus Neupert, “Finite-momentum cooper pairing in proximitized altermagnets,” *Nature Communications* **15**, 1801 (2024).
- [54] Sayan Banerjee and Mathias S. Scheurer, “Altermagnetic superconducting diode effect,” *Phys. Rev. B* **110**, 024503 (2024).
- [55] Mercè Roig, Andreas Kreisel, Yue Yu, Brian M. Andersen, and Daniel F. Agterberg, “Minimal models for altermagnetism,” *Phys. Rev. B* **110**, 144412 (2024).
- [56] Niclas Heinsdorf, “Altermagnetic instabilities from quantum geometry,” *Phys. Rev. B* **111**, 174407 (2025).
- [57] Xingchuan Zhu, Xingmin Huo, Shiping Feng, Song-Bo Zhang, Shengyuan A. Yang, and Huaiming Guo, “Design of altermagnetic models from spin clusters,” *Phys. Rev. Lett.* **134**, 166701 (2025).
- [58] Liang Fu and C. L. Kane, “Superconducting proximity effect and majorana fermions at the surface of a topological insulator,” *Phys. Rev. Lett.* **100**, 096407 (2008).
- [59] Catherine Kallin and John Berlinsky, “Chiral superconductors,” *Reports on Progress in Physics* **79**, 054502 (2016).
- [60] Rafael González-Hernández, Libor Šmejkal, Karel Výborný, Yuta Yahagi, Jairo Sinova, Tomáš Jungwirth, and Jakub Železný, “Efficient electrical spin splitter based on nonrelativistic collinear antiferromagnetism,” *Phys. Rev. Lett.* **126**, 127701 (2021).
- [61] Paul A. McClarty and Jeffrey G. Rau, “Landau theory of altermagnetism,” *Phys. Rev. Lett.* **132**, 176702 (2024).
- [62] O. J. Amin, A. Dal Din, E. Golias, Y. Niu, A. Zakharov, S. C. Fromage, C. J. B. Fields, S. L. Heywood, R. B. Cousins, F. Maccherozzi, J. Krempaský, J. H. Dil, D. Kriegner, B. Kiraly, R. P. Campion, A. W. Rushforth, K. W. Edmonds, S. S. Dhesi, L. Šmejkal, T. Jungwirth, and P. Wadley, “Nanoscale imaging and control of altermagnetism in MnTe ,” *Nature* **636**, 348–353 (2024).
- [63] Michael Tinkham, *Introduction to superconductivity* (Dover Publications, 2004).
- [64] E. B. Rosa and L. Cohen, “On the self-inductance of circles,” *Bulletin of the Bureau of Standards* **4**, 149 (1907).
- [65] Pengcheng Dai, “Antiferromagnetic order and spin dynamics in iron-based superconductors,” *Rev. Mod. Phys.* **87**, 855–896 (2015).
- [66] Christian Pfleiderer, “Superconducting phases of f -electron compounds,” *Rev. Mod. Phys.* **81**, 1551–1624 (2009).
- [67] Dai Aoki, Kenji Ishida, and Jacques Flouquet, “Review of u -based ferromagnetic superconductors: Comparison between Uge_2 , Urhge , and Ucoge ,” *Journal of the Physical Society of Japan* **88**, 022001 (2019).
- [68] Debmalya Chakraborty and Annica M. Black-Schaffer, “Zero-field finite-momentum and field-induced superconductivity in altermagnets,” (2024), [arXiv:2309.14427 \[cond-mat.supr-con\]](https://arxiv.org/abs/2309.14427).
- [69] Daniel E. Sheehy, T. P. Davis, and M. Franz, “Unified theory of the ab -plane and c -axis penetration depths of underdoped cuprates,” *Phys. Rev. B* **70**, 054510 (2004).

- [70] Tarun Tummuru, Stephan Plugge, and Marcel Franz, “Josephson effects in twisted cuprate bilayers,” [Phys. Rev. B **105**, 064501 \(2022\)](#).